Electrochemical Energy Reviews (2023) 6:26
https://doi.org/10.1007/s41918-023-00183-9

REVIEW ARTICLE

Ion Exchange Membranes in Electrochemical CO_2 Reduction Processes

Faezeh Habibzadeh[1,2] · Peter Mardle[1,3] · Nana Zhao[1] · Harry D. Riley[1] · Danielle A. Salvatore[4] · Curtis P. Berlinguette[2,4,5,6] · Steven Holdcroft[3] · Zhiqing Shi[1]

Received: 3 May 2022 / Revised: 3 November 2022 / Accepted: 28 February 2023 / Published online: 27 July 2023

Abstract

The low-temperature electrolysis of CO_2 in membrane-based flow reactors is a promising technology for converting captured CO_2 into valuable chemicals and fuels. In recent years, substantial improvements in reactor design have significantly improved the economic viability of this technology; thus, the field has experienced a rapid increase in research interest. Among the factors related to reactor design, the ion exchange membrane (IEM) plays a prominent role in the energetic efficiency of CO_2 conversion into useful products. Reactors utilizing cation exchange, anion exchange and bipolar membranes have all been developed, each providing unique benefits and challenges that must be overcome before large-scale commercialization is feasible. Therefore, to direct advances in IEM technology specific to electrochemical CO_2 reduction reactions (CO_2RRs), this review serves to first provide polymer scientists with a general understanding of membrane-based CO_2RR reactors and membrane-related shortcomings and to encourage systematic synthetic approaches to develop membranes that meet the specific requirements of CO_2RRs. Second, this review provides researchers in the fields of electrocatalysis and CO_2RRs with more detailed insight into the often-overlooked membrane roles and requirements; thus, new methodologies for membrane evaluation during CO_2RR may be developed. By using CO_2-to-CO/$HCOO^-$ methodologies as practical baseline systems, a clear conceptualization of the merits and challenges of different systems and reasonable objectives for future research and development are presented.

Keywords Ion exchange membranes · CO_2 electrolysis · Electrochemical CO_2 reduction · Membrane-based CO_2 electrolyzer · Carbon capture and utilization

✉ Steven Holdcroft
holdcrof@sfu.ca

✉ Zhiqing Shi
Zhiqing.Shi@nrc-cnrc.gc.ca

1 Energy, Mining and Environment Research Center, National Research Council Canada, 4250 Wesbrook Mall, Vancouver, BC V6T 1 W5, Canada

2 Department of Chemistry, The University of British Columbia, 2036 Main Mall, Vancouver, BC V6T 1Z1, Canada

3 Department of Chemistry, Simon Fraser University, 8888 University Drive, Burnaby, BC V5A 1S6, Canada

4 Department of Chemical and Biological Engineering, The University of British Columbia, 2360 East Mall, Vancouver, BC V6T 1Z3, Canada

5 Stewart Blusson Quantum Matter Institute, The University of British Columbia, 2355 East Mall, Vancouver, BC V6T 1Z4, Canada

6 Canadian Institute for Advanced Research (CIFAR), 661 University Avenue, Toronto, ON M5G 1M1, Canada

1 Introduction

To meet the 2015 Paris Agreement requirement of limiting global warming to 1.5 °C, net zero greenhouse gas (GHG) emissions must be achieved by 2050. Due to globally rising energy demands, any strategy for meeting these goals must include carbon capture and sequestration (CCS) technologies, such as storing CO_2 underground [1, 2]. However, utilizing the captured CO_2 [i.e., carbon capture and utilization (CCU)] serves as an attractive and potentially economical alternative to CCS [3, 4]. The petrochemical industry comprises approximately 10% of all GHG emissions, 80% of which are directly related to the sourcing and refining of feedstock chemicals from fossilized carbon sources [5–7]. The electrochemical CO_2 reduction reaction (CO_2RR) provides an alternative method for sourcing these feedstock chemicals from captured CO_2 gas to form various products, such as carbon monoxide, methane, formic acid, ethanol and,

in particular, ethylene, which is used to manufacture common plastics [8].

The electrochemical CO_2RR was introduced in the mid-1900s to produce formate ($HCOO^-$) with electrochemical cells comprising Hg cathodes immersed in CO_2-saturated aqueous solutions [9]. Processes have typically been performed in a two-compartment cell configuration, where electrode chambers are separated by a porous diaphragm [10]. The diaphragm was replaced by a cation exchange membrane (CEM) in the late 1960s/early 1970s, increasing formate production efficiency from 25% to 78% by limiting the crossover of the product [11]. In the 1980s, commodity products other than formate were prioritized, e.g., methanol. Notably, Hori and coworkers [12–16] discovered the unique CO_2RR selectivity to higher order carbon on Cu and published a seminal review that sparked significant research activity on selective electrocatalysis for different CO_2RR products [17]. For more on the topic of CO_2RR electrocatalysts, the reader is referred to one of several reviews [18–23].

In recent years, research into novel CO_2RR device configurations, including the incorporation of gas diffusion electrodes (GDEs) to increase the mass transport of reactant CO_2 and the development of various device configurations has increased the current densities of CO_2RR reactors from 100 μA cm^{-2} to > 500 mA cm^{-2} [24, 25]. Coupled with previous advances in electrocatalyst development, product selectivity has reached 95%. These conversion metrics have propelled electrochemical CO_2RR to be a potentially economically viable carbon utilization technology, garnering the attention of a wide field of electrochemical engineers and scientists [26–37].

Considering the energy requirements of external systems such as CO_2 capture, thermal management and product separation are critical for economically viable CO_2RR. For example, coupling CO_2 utilization with the on-site capture of flue gas considerably reduces costs for the complete system by avoiding the external capture, compression and transportation of CO_2 [38]. Nevertheless, the most important metric on the single-cell level is energetic efficiency (EE), which is defined as the ratio of energy consumption for the production of a given product to the total electrical energy input of the CO_2 reactor:

$$\mathrm{EE} = \frac{\mathrm{FE}_i \times E_i^{0'}}{E_{\mathrm{cell}}} \times 100 \quad (1)$$

where FE_i is the Faradaic efficiency at which product i is produced, $E_i^{0'}$ is the thermodynamic equilibrium potential of the overall reaction to produce i, and E_{cell} is the voltage of the cell.

The cell voltage (E_{cell}) is the sum of cathodic and anodic thermodynamic potentials and the associated overpotentials required for overcoming kinetic, concentration, and ohmic resistances. The total ohmic resistance of a cell is a combination of the ionic and electronic resistances. Of the two resistance values, the ionic resistance contributes more and is governed by the ionic conductance of the electrolyte and/or membrane.

Faradaic efficiency (FE) reflects the selectivity of the CO_2RR toward a particular product, and it is defined as the ratio of the number of electrons consumed to generate the product to the total number of electrons passing for a given duration of electrolysis. High FE is critical for capital and operating costs as it reduces the number of postproduction separation steps.

The objective of industrial CO_2RRs is to develop electrochemical cells that maximize the EE for a singular product by maximizing the FE at the lowest possible E_{cell} value. The EE values of recent CO_2 electrolyzers are typically < 50% [39], which are much lower than those of modern alkaline water electrolyzers (> 70%) [40] and far below that required to consider the electrolyzer economically viable. Calculations by Martin et al. show that to achieve an EE of 60% and an FE of 90% for the production of CH_3OH and CO, the maximum total overvoltage values allowed are 600 and 700 mV, respectively [39]. These overvoltage values are typically exceeded even under low current densities. Therefore, despite recent advances promising potential economic viability, further improvement in electrocatalysis, GDE configuration and reactor design is needed. Furthermore, techno-economic analyses have shown that the economic viability for high-order products, such as ethylene and ethanol, is only theoretically achievable with an abundant source of inexpensive electricity (typically < \$0.05 kW h^{-1}), requiring the proliferation of renewable energy sources [8, 41–43].

Electrochemical CO_2RR reactors (CO_2 electrolyzers) are electrolytic devices in which the reduction in CO_2 at the cathode is balanced by a complementary oxidation reaction at the anode, typically the oxygen evolution reaction (OER) or other reactions with lower reduction potentials [44, 45]. An external electricity source is used to generate potential differences at the electrode/electrolyte interfaces and between the electrodes, driving electrochemical reactions. The resultant electrical current is maintained by the transport of ions in a liquid or a solid electrolyte that separates the electrodes. In devices without solid barriers separating the cathode and the anode compartments (i.e., membraneless or microfluidic reactors, Fig. 1a) [32], the flow of current between the electrodes is mediated by the movement of ions in a liquid electrolyte. Scaling up membraneless or microfluidic reactors poses a significant challenge as the cross-interaction between the anodic and cathodic half-reactions increases with the size of the reactor [46]. However, electrolyzers that employ a solid electrolyte membrane to separate electrodes

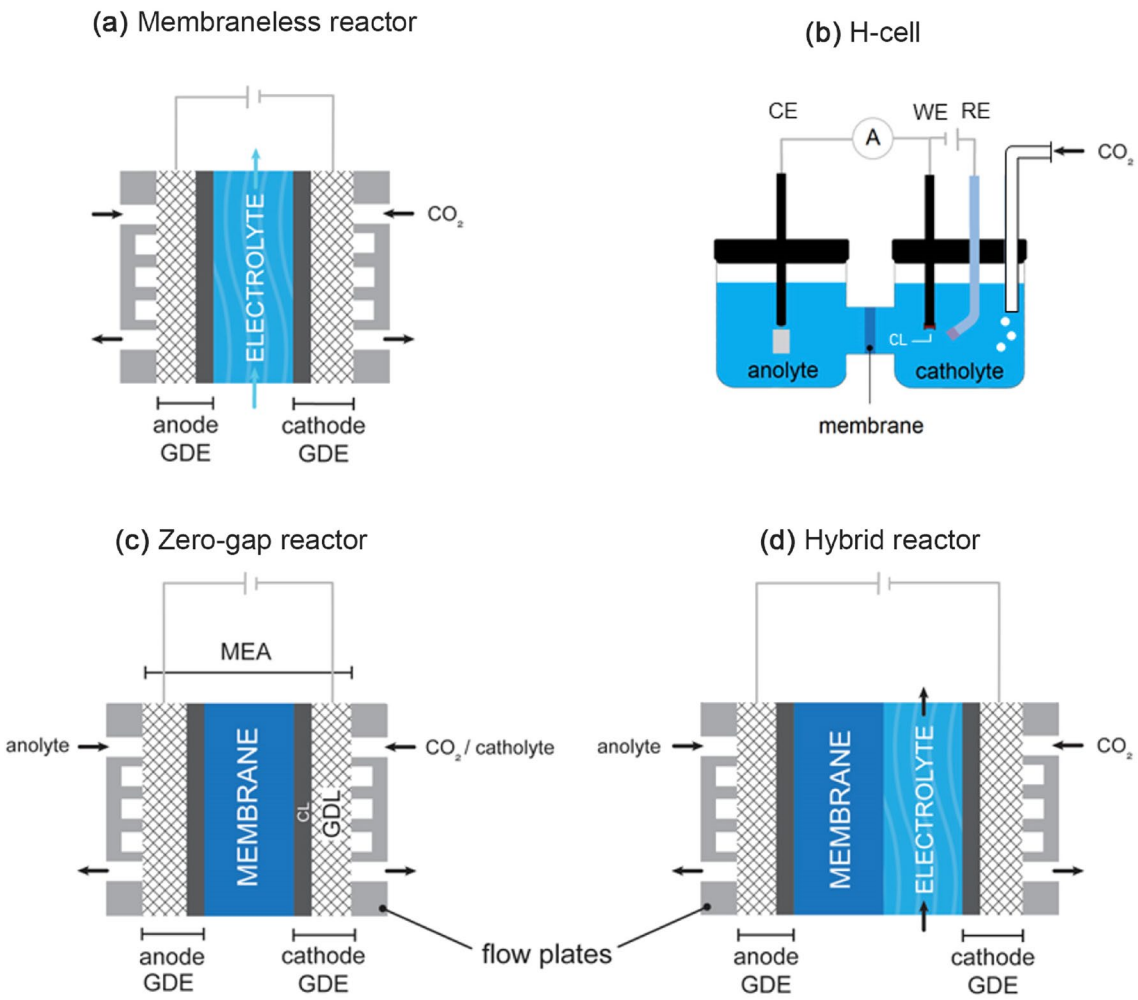

Fig. 1 Diagrams of different cell configurations used for CO_2RR (solid oxide electrolyzers are excluded). **a** Membraneless electrolyzer and three types of membrane-based reactors; **b** batch-type H-cell, where CE, WE and RE represent the counter, working and reference electrodes, respectively; **c** zero-gap electrolyzer; and **d** hybrid flow electrolyzer. MEA represents the membrane-electrode assembly, which consists of the membrane, the cathode GDE, and the anode GDEs. GDEs typically consist of a carbon-based gas diffusion layer (GDL) containing a catalyst layer (CL)

(i.e., membrane-based reactors) circumvent product mixing to a degree and are amenable to scale-up processes.

Concerning only the reactors that employ an ion exchange membrane (IEM), two main categories can be defined based on the presence or absence of the forced flow of reactants and products.

(1) H-cells are batch-type electrochemical cells named after their shape; the anodes and cathodes in their respective electrolyte chambers are separated by a membrane (Fig. 1b). CO_2RR electrocatalysts are deposited on a conductive substrate and contact a solution saturated with CO_2 (catholyte). In the anode compartment, the anode is submerged in an electrolyte solution (anolyte) that is potentially identical to the catholyte. Due to the simplicity of incorporating a reference electrode near the cathodic CO_2RR electrode, H-cells are ideal for laboratory-scale, fundamental studies of half-reactions, and provide powerful tools for obtaining mechanistic information about CO_2RR using different catalysts [47]. The main disadvantage of H-cells arises from the low solubility of CO_2 in aqueous solutions (~33 mM at standard temperature and pressure, 1 M = 1 mol L^{-1}), limiting the steady-state current density of batch reactors to ~10 mA cm^{-2} [48]. Moreover, H-cell batch reactors typically suffer from high ohmic losses due to the large distance between the cathode and the anode, limiting their applicability for industrial electrolysis.

(2) Flow reactors operate under the continuous circulation of cathodic and anodic feedstocks. In membrane-based flow reactors, the IEM separates the porous anode and cathode that are positioned parallel to each other. Both liquid and gaseous feedstocks could be fed to the electrodes. In gas-fed flow reactors, the forceful flow of concentrated gaseous

CO_2 streams through pores within the cathode reduces mass transport issues and significantly increases the total current densities [28]. Operational parameters, such as the flow rate, temperature, and pressure of the reactants, can be adjusted to maximize the performance. Moreover, membrane reactors can be stacked, which makes them attractive for industrial applications.

Membrane-based flow CO_2RR reactors are available in two configurations: zero-gap reactors and hybrid reactors. In zero-gap reactors (Fig. 1c), conductive cathode and anode flow plates tightly sandwich a membrane-electrode assembly (MEA). The MEA consists of cathode and anode gas diffusion electrodes (GDEs) situated against each side of the IEM with their catalyst layers (CLs) in direct contact with the membrane. This configuration enhances the mass transport of reactant species to the reaction interfaces, increasing conversion rates. Moreover, zero-gap reactors experience reduced ohmic drops due to the minimized distance between the cathode and anode.

In a hybrid reactor, a layer of the electrolyte solution (catholyte) circulates between the cathode GDE and the membrane; therefore, the cathode CL and the membrane are not in direct contact (Fig. 1d). This configuration is commonly used when a buffer layer adjacent to the cathode catalyst layer is required to maintain a neutral to mildly alkaline pH desirable for the selective production of some CO_2RR products [49, 50]. Hybrid reactors are good candidates for comparing the performance levels of different GDEs and electrocatalysts when energy losses due to ohmic resistance are not a concern [51].

2 Recent Status of IEM-Based CO_2RR Reactors

Low-temperature CO_2 electrolysis with a commercial polymer membrane, either in batch-type (H-cell) or flow cell reactor architectures, has shown rapid growth within recent years (Fig. 2a). Cation exchange membranes (CEMs) have been used mostly in batch-type reactors (Fig. 2b), which are the primary reactor of choice for fundamental mechanistic studies of newly developed electrocatalysts. Since most CO_2RR research focuses on catalyst design and tuning the selectivity in H-cells that typically utilize CEMs, the number of reports of CEMs in CO_2RR studies have dominated early research and is continuously increasing to date. This increasing trend includes the more recent use of CEMs in flow reactors, where novel reactor designs help with overcoming some of the inherent challenges associated with CEMs, namely, the flux of protons toward the cathode during continuous electrolysis favoring the formation of hydrogen over the CO_2RR.

To overcome challenges associated with CEMs, anion exchange membranes (AEMs) have emerged gradually (Fig. 2a) as alternative membranes in CO_2RR electrolysis, especially when alkaline conditions are desired. This growth corresponds to significant developments toward various alkaline stable and conductive AEM materials, which have previously been a significant challenge in early anion exchange membrane fuel cell systems [52]. These advances have significantly increased interest in AEMs as an alternative to CEMs in water electrolyzers [53]. AEMs are more popular choices than CEMs for use in flow CO_2 electrolyzers (Fig. 2b); many of the recent state-of-the-art IEM-based flow CO_2RR reactors are AEM-based (Table 1).

A new class of IEMs used for CO_2RRs is bipolar membranes (BPMs), which were first introduced to the field in 2016 for gas-phase CO_2RRs [36, 54]. BPMs are fabricated by laminating a cation exchange layer (CEL) and an anion exchange layer (AEL). Cationic and anionic mobile counterions are transported through their respective segments and either combine to form water (forward bias, i.e., CELs at the anodes) or transport from the interface, where subsequent electric potential facilitates the rapid dissociation of water through the second Wien effect (reverse bias, i.e., CELs at the cathodes) [55]. This effect is typically aided by the presence of catalysts at the interface of the BPM [56, 57]. BPMs have increased in attention, particularly after the reporting of BPM-based flow reactors using liquid bicarbonate as the feedstock in 2019 [58].

Considering the different CO_2RR schemes, low-temperature CO_2 electrolysis in flow reactors that utilize IEMs is an attractive option offering potential scale-up and control of product selectivity [59]. However, despite advances in the catalytic and configurational design of CO_2RR reactors, less effort has been devoted to advancing IEMs for CO_2RRs. Recently, Salvatore et al. have addressed the principles, desired properties, and challenges associated with commercially available AEMs for CO_2RR applications [60]. However, primarily due to product and carbonate ion crossover through AEMs, CEMs and BPMs remain under investigation. Lees et al. have recently discussed both GDEs and IEMs for CO_2RRs and the inherent advantages and disadvantages of various configurations [24]. From these contributions and the status of the field, it is clear that IEM development requires a specific focus on their applications in CO_2RRs. This paper serves to guide these efforts with a more comprehensive focus on three categories of IEMs, highlighting the key properties affecting the performance metrics of CO_2RR reactors. By using a CO_2RR to generate

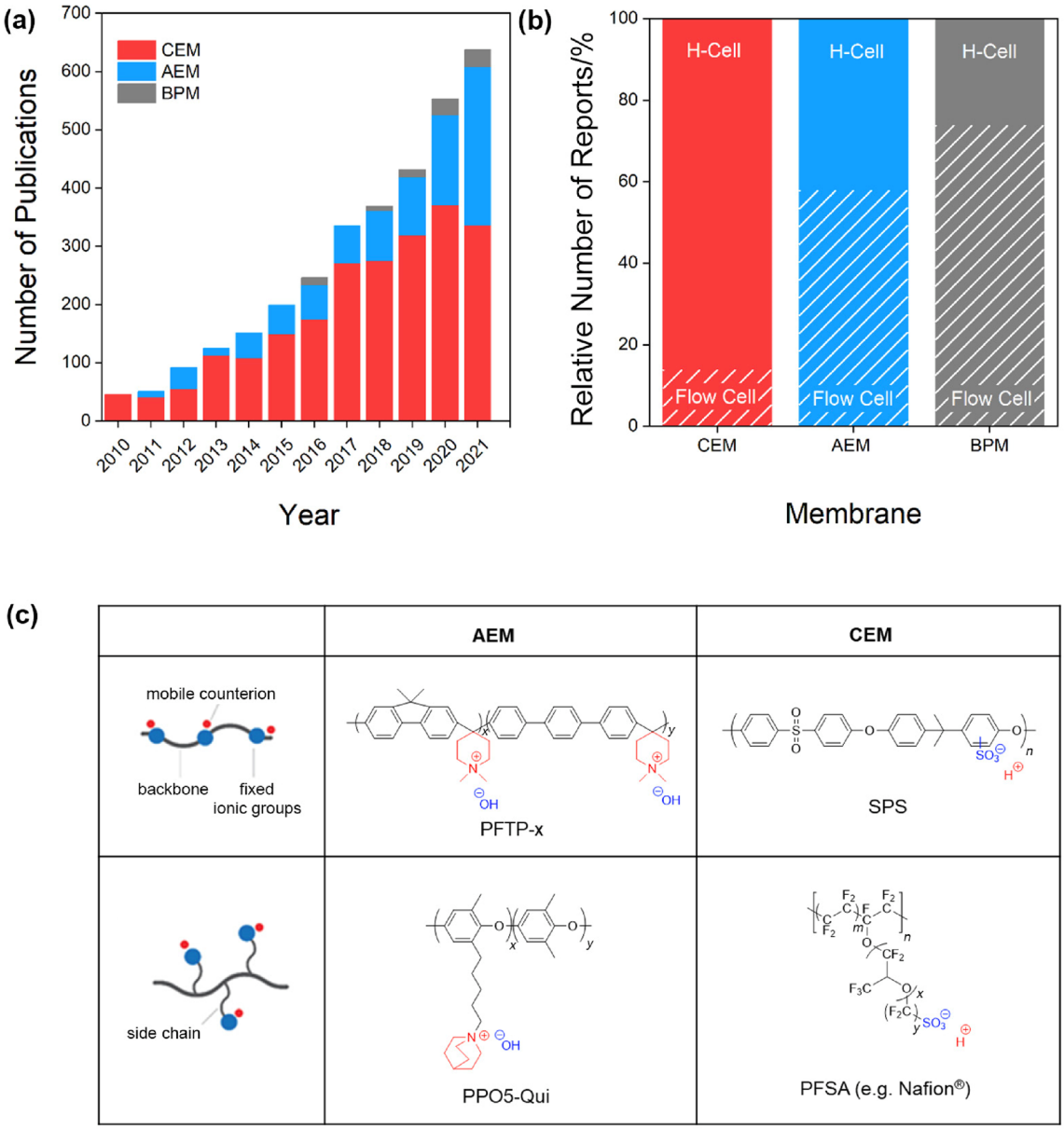

Fig. 2 Infographic analysis of 3 237 literature reports published from 2010 to 2021 (source: Web of Science) on electrochemical CO_2 reduction in aqueous systems using commercial IEMs. **a** Number of publications per annum, categorized by the type of membrane used. **b** Percentages of commercial IEMs used in flow (dashed) and H-cell (solid) CO_2 electrolyzers. **c** Examples of two classes of ion exchange polymers with different arrangements of functional groups: ionic groups placed directly on the backbone (i.e., ionenes) with examples poly(fluorene-co-terphenyl *N,N′*-dimethyl-piperidinium) (AEM) [61] and sulfonated polysulfone (CEM) [62]; ionic groups placed on side chains attached to the backbone with examples quinuclidine-functionalized polyphenylene oxide (AEM) [63] and perfluoro sulfonic acid (CEM) [64]

C_1 products (CO or $HCOO^-$) as a baseline system, property–performance correlations are discussed regarding energetic efficiency (separating cell voltage and Faradaic efficiency) and device stability. Targets for IEM development are proposed for each category to expedite the adoption of this critical technology for future energy systems.

3 IEMs for CO_2RR

The primary roles of membranes in electrochemical applications are (1) to provide an electronic barrier between the cathode and anode to prevent short-circuiting; (2) to act as a physical barrier to facilitate the elimination of compartmental cross-contamination; and (3) to maintain ionic connectivity between the catholyte and anolyte compartments

Table 1 Some state-of-the-art performance metrics of flow CO_2RR electrolyzers using different types of IEMs

IEM	IEM type	Cathode feed	Anode feed	Base metal of CO_2RR catalyst	E_{cell}/V	Main product (FE/%)	Total current density[a]/(mA cm^{-2})	Stability	Ref.
Nafion™ 117	CEM	CO_2 + 2 M $KHCO_3$	2 M KOH	Ag	3.9–4.9	CO (90)	220	10 h, r. t.[b]	[65]
Nafion™ 117	CEM	CO_2 + 2 M KCl	2 M KOH	Cu	3.30	C_{2+} (80)	150	30 h, r. t	[66]
Nafion™ 212	CEM	Dry CO_2	Humidified H_2	Sn	2.47	HCOOH (72)	385	1 h, r. t	[67]
PiperION TP-85	AEM	Humidified CO_2	0.1 M CsOH	Ag	3.20	CO (85)	> 1 000	100 h (60 °C)	[46]
Aemion™ AF1-CNN8-60-X	AEM	Humidified CO_2	0.1 M $KHCO_3$	Cu	3.75	$CH_3OH + C_3H_7OH$ (–)	150	100 h (40 °C)	[68]
Sustainion® X37-50	AEM	Humidified CO_2	0.01 M $KHCO_3$	Ag	2.89	CO (99)	100	> 3 000 h	[69]
Selemion™ DSVN	AEM	CO_2 + 1 M $KHCO_3$	1 M $KHCO_3$	Ni	–	CO (98)	400	30 h	[70]
QAPPT	AEM	CO_2 + 10 mM CsOH	10 mM CsOH	Ag	3.3	CO (90)	550	100 h	[25]
Fumasep® FBM	BPM	3 M $KHCO_3$	1 M KOH	Ag	3.5	CO (82)	100	8 h, r. t	[71]
Fumasep® FBM-PK	BPM	CO_2 (40 bar[c]) + 0.5 M $KHCO_3$	1 M KOH	Sn	3.5	HCOOH (90)	30	1/3 h, r. t	[72]

[a]Geometric current density;

[b]Room temperature;

[c]1 bar = 100 kPa

via ion transportation. Polymeric IEMs are based on polymers bearing immobilized ion exchange groups which hold mobile counterions that move freely within the matrix of a membrane. The incorporation of ionic exchange groups along the polymer chains is achieved by their direct integration either into the main chain or into the appendage as a side chain (Fig. 2c) [62, 73]. Based on the types of ionic functional groups attached to the polymer chains, IEMs are classified into CEMs and AEMs. CEMs, as discussed in Sect. 3.1, are membranes based on polymers with fixed negatively charged ions, such as sulfonate, phosphonate and sulfonamide groups; they provide mobility for counter cations, such as H^+, Na^+, and K^+. AEMs possess fixed positively charged ions, such as $–NH_3^+$, $–NRH_2^+$, $–NR_2H^+$ and $–NR_3^+$ (R = hydrocarbon chain) cations, allowing for the mobility of counteranions (e.g., OH^-, CO_3^{2-}, HCO_3^-); they are discussed in Sect. 3.2. A CEM and an AEM can be laminated together to form a new class of membranes called BPMs, which are reviewed in Sect. 3.3.

3.1 CEMs

For CO_2RR applications, CEMs are mostly used to separate anodic and cathodic compartments in batch-type (H-cell) reactors filled with CO_2-saturated aqueous electrolytes, aiding catalyst development. The efficient conversion from CO_2 to products, such as CO (> 97% FE) [74], HCOOH (> 98% FE) [75], CH_4 (85% FE) [76], and alcohols (63% overall FE for ethanol + *n*-propanol) [77], has been achieved in batch-type reactors by using Nafion™ CEMs in near-neutral to alkaline pH conditions (pH 7–8). To a lesser extent, CEMs have been used in flow reactors [78, 79]. In a zero-gap configuration, shown in Fig. 3a, the application of CEMs mirrors the work conducted in proton exchange membrane (PEM) fuel cells and PEM water electrolyzers. Due to their ability to inhibit anionic product crossover, CEMs are primarily used in flow electrolyzers that convert CO_2 to anionic formate ($HCOO^-$) (see Sect. 4). However, novel cell designs that leverage the high proton conductivity of CEMs to reduce ohmic losses during the conversion from CO_2 to CO have been reported. Recently, Zhang et al. have utilized Nafion™ membranes to mediate the transport of protons produced via the oxidation of H_2 gas at the anode of a flow cell [80]. The H^+ transported to the cathode by Nafion™ enables the conversion from bicarbonate into electrochemically active CO_2, which further reduces to CO. Using this configuration, the remarkably low cell voltage of 2.3 V is achieved at a high CO partial current density of 220 mA cm^{-2}. Another effective and more common configuration for CO_2 electrolyzers with CEMs that produces CO as the main product is shown in Fig. 3b, where a buffer layer of electrolyte circulates between the CEM and the cathode. This hybrid cell structure enables the adjustment of the catholyte pH, which is used to suppress the hydrogen evolution reaction (HER).

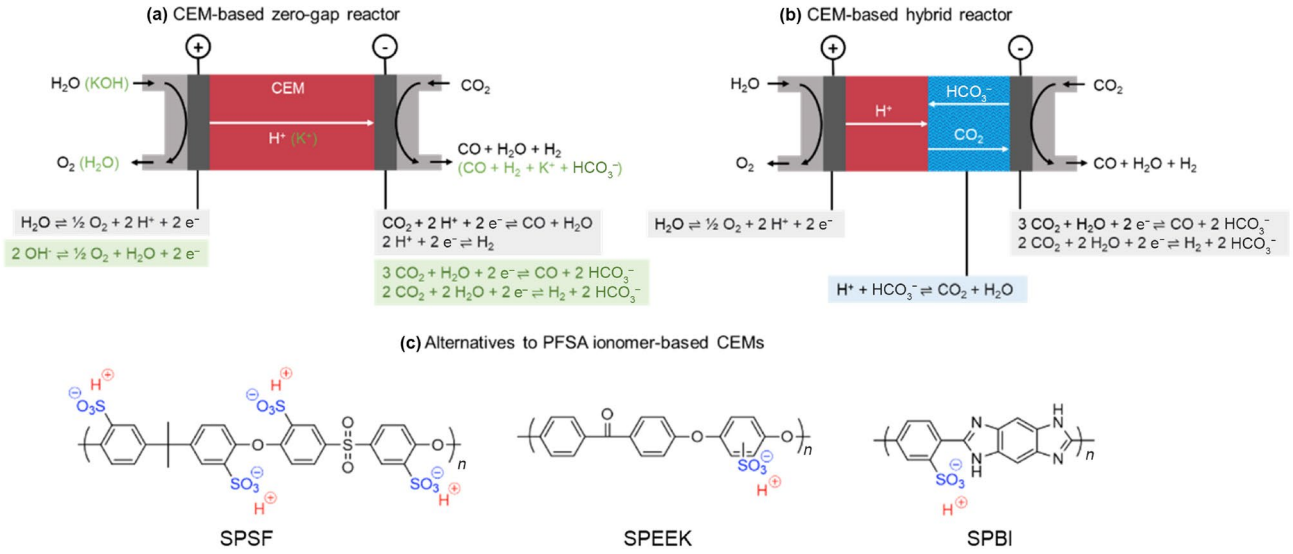

Fig. 3 Designs for CEM-based CO_2 electrolyzers in **a** zero-gap and **b** hybrid configurations. The green text in (**a**) depicts the alternative electrochemical reactions when KOH is fed to the anode instead of water. The text in blue in (**b**) represents the chemical acid–base reactions occurring in the adjacent catholyte layer. **c** Chemical structures of some nonfluorinated alternatives to perfluorinated sulfonic acid (PFSA) ionomer-based membranes

This reaction readily occurs under the acidic conditions provided by the CEM. However, this modification is associated with energy losses due to the ohmic resistance imposed by the addition of a buffer solution.

The most prominent family of CEMs features PFSA ionomer-based membranes (e.g., Nafion™, shown in Fig. 2c) that are widely employed in CO_2RR reactors. However, Nafion™ membranes are expensive, operate at limited temperatures (< 100 °C), suffer from excessive swelling when high concentrations of alcohols are present and are under increasing scrutiny due to toxicity concerns [81]. In addition to Nafion™, other commercially available PFSA-based CEMs, such as Aquivion™ (Solvay, Belgium) and Fumasep® or Fumapem® (Fumatech, Germany), have been employed for CO_2RRs. In addition, applications of reinforced PFSA membranes have been reported in pressurized CO_2 (50–150 bar) flow reactors [51, 82, 83].

Besides CO_2RR applications, nonfluorinated CEMs based on sulfonated poly(ether ether ketone) (SPEEK), sulfonated polysulfone (SPSF), phosphoric acid-doped polybenzimidazole (PBI) and sulfonated polybenzimidazole (SPBI) are introduced as alternatives to Nafion™ for applications in high-temperature fuel cells (Fig. 3c) [84]. Due to their aromatic structures, these polymers improve the mechanical strength and thermal stability characteristics of CEMs. Comparatively, examples of novel CEMs exclusively designed for CO_2RR are scarce. In a work by Gutiérrez-Guerra et al., polybenzimidazole (PBI) membranes are doped with H_3PO_4 to enhance their conductivity and help them sustain high-temperature CO_2 electrolysis (110 °C) [85]. By feeding CO_2 to a flow reactor with H_3PO_4/H_2O as the anodic solution and a copper-based cathode catalyst, a series of multicarbon products form. Under these conditions, FE values are, however, low (< 2%) for all products, and HER is the dominant cathodic process; these phenomena are expected with acidic reaction environments. Nonetheless, as discussed in the following sections, the high ionic conductivity and low anionic product crossover of CEMs encourage their further development for CO_2RRs.

3.1.1 Proton Conductivity

When current passes through an IEM-based electrolysis system, the flow of charge within the membrane is mediated by the movement of mobile counterions, such as H^+ or OH^- in CEMs and AEMs, respectively. The flux, i.e., the directional transport rate of ion i (J_i, mol s^{-1} cm^{-2}) in an IEM under steady-state conditions, is governed by a combination of diffusion, migration, and convection mass transport phenomena, as described by the Nernst–Planck equation [Eq. (2)] [86]:

$$J_i = -D_i\frac{\Delta C_i}{\Delta x} + C_i v - \frac{z_i F}{RT}D_i C_i\frac{\Delta \phi}{\Delta x}, i = \mathrm{H^+},\ \mathrm{OH^-} \qquad (2)$$

where D_i (cm^2 s^{-1}) is the diffusion coefficient of ion i in the membrane; C_i (mol cm^{-3}) is the concentration of i in the membrane; ΔC_i (mol cm^{-3}) is the difference in the

concentration of ion i across the thickness of the membrane (Δx, cm); $\Delta\phi$ (V) is the electrical potential difference across the membrane; v (cm s^{-1}) is the linear velocity of ions when advection is induced by a momentum gradient across the membrane; z_i is the charge of ion i; and F/RT is a constant at a given temperature (e.g., 38.9 V^{-1} at 25 °C).

The first term in Eq. (2) corresponds to ion diffusion. The tortuosity and electrostatic interaction effects of the polymer hinder the movement of counterions within the membrane matrix relative to the movement of the ions in the solution reducing the diffusion coefficients of the ions in the membrane [87]. The effective diffusion coefficient of the charged species in the membrane may be calculated by using the ion diffusion coefficient in water while accounting for parameters related to the IEM, such as the density, equivalent weight, and tortuosity [88, 89]. The second term in Eq. (2), $C_i v$, represents the advection or hydraulic transport of ions due to pressure gradients across the membrane. Under electrolysis conditions, the contributions of diffusion and advection to the net ion transport in the membrane are considerably smaller than that of electromigration $\left(-\frac{z_i F}{RT} D_i C_i \frac{\Delta\phi}{\Delta x}\right)$ [86]. The electromigration of charged species defines the ionic conductivity and conductance [89] and the potential [86] of the membrane and is predominantly influenced by the ion exchange capacity, ionic channel contiguousness, and water uptake (WU) of the membrane.

Equation (2) typically invokes the concept of vehicular ion transport under the gradient of a driving force (i.e., the concentration, potential, and pressure gradients for diffusion, migration, and convection, respectively). However, other mechanisms of mobility exist in IEMs, such as the surface mechanism (i.e., the direct transport via polymer chain segmental motions) and, more importantly, the Grotthuss mechanism for the transport of protons [90]. The prevalence of each mechanism (vehicular, surface or Grotthuss) depends on the hydration level of the membrane [91]. At low water contents, the ratio of the surface to the bulk water increases, and the surface mechanism by which counterions directly transport between neighboring fixed functional groups on hydrophilic channel walls becomes increasingly significant [92]. This mode of transport has a high activation energy and is not considered the main mechanism of ion transport for high hydration levels, where vehicular and Grotthuss mechanisms dominate. In CEMs, the Grotthuss mechanism specifically applies to the transport of protons, which hop from one hydrolyzed anionic site to another via the formation of hydronium ions (Fig. 4a). This process is much faster than the vehicular transport of alkali metal ions; therefore, it is more favorable to transport H^+ than other cationic species [64].

To improve the conductivities of membranes, a key property to change is the ion exchange capacity (IEC, meq g^{-1}). The IEC is the inverse of the equivalent weight (EW) and refers to the densities of ionic charges within the membrane. In addition to an increased concentration of ionic charges, a high IEC typically benefits the ionic conductivity of membranes through an increase in the water content. Figure 4b shows the linear relationship between the IEC (1/EW) and conductivity for various commercialized perfluorosulfonated ionomers (PFSAs). Additionally, relative to the comparatively low IECs of non-PFSA alternatives, PFSAs such as Nafion^{TM} exhibit high proton conductivities of > 100 mS cm^{-1} (Fig. 4c). This phenomenon occurs due to the phase separation of the hydrophobic perfluorinated backbone and the hydrophilic pendant groups, resulting in a highly percolating network of hydrated ion channels [64].

3.1.2 Cation Crossover and CO_2RR Selectivity

In CO_2RR electrochemical cells, CEMs are often operated with $KHCO_3$ or K_2CO_3 electrolyte, where the concentration of K^+ in the solution is several orders of magnitude higher than that of H^+. Under these conditions, K^+ ions diffuse extensively in the membrane [30]. The cotransport of alkali metal cations, such as K^+ relative to H^+, in a CEM is correlated to its relative permeability and diffusion coefficient; the diffusion coefficient is inversely related to the hydrated radius (diffusion coefficient order: $Cs^+ > K^+ > Na^+ > Li^+$) [94]. The selective transport of alkali metal cations through the CEM can be leveraged to enhance the cation-induced selectivity. Liao et al. have substituted H^+ in Nafion^{TM} XL membranes with the previously mentioned series of alkali cations [95]. The highest FE for the CO_2RR (0.44%) is measured for the membrane in the Cs^+ cation form and is attributed to a decrease in proton transport through the CEM because of a decrease in membrane water uptake (Fig. 5a). Leaching of the substituted cations to the cathode is observed by postmortem elemental analysis; thus, enhancements can occur due to the activation of the CO_2RR at the cathode by the cations. Sargent et al. have shown that by positioning a K^+-saturated cation exchange layer next to a copper cathode, a single-pass carbon utilization efficiency (i.e., the percent of carbon converted to useful products) of 77% can be achieved in a flow reactor with an acidic electrolyte (1 M H_3PO_4 + 3 M KCl, pH ≈ 1, Fig. 5b, c) [96]. This selectivity greatly increases by activating the CO_2RR through the presence of alkali cations, where changes in the electric field density favorably enhance the strength of CO_2 adsorption and thus the CO_2RR kinetics (Fig. 5d) [97, 98]. Nevertheless, under the acidic environment provided by the CEM, HER remains a competing reaction, causing FE to be typically < 80% for C_1 products.

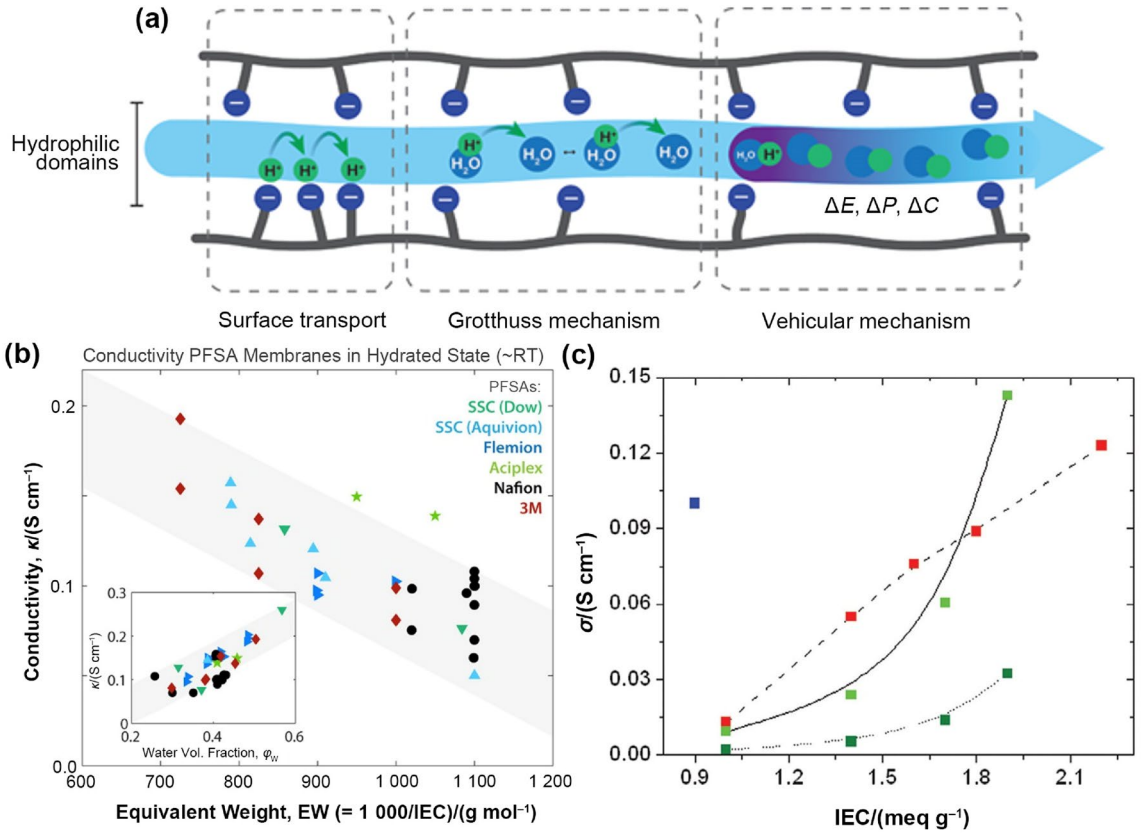

Fig. 4 **a** Modes of proton transport in a CEM: surface, Grotthuss, and vehicular transport driven by the potential gradient (ΔE), pressure (momentum) gradient (ΔP), and concentration gradient (ΔC), respectively. **b** Proton conductivities of various PFSA-based CEMs as functions of the equivalent weight and the water volume mole fraction. Reproduced with permission from Ref. [64]. Copyright © 2017, American Chemical Society. **c** Proton conductivity (σ) of Nafion^{TM} (blue) as a function of IEC relative to non-PFSA alternatives, such as sulfonated polyphenylenes (red). Reproduced with permission from Ref. [93]. Copyright © 2010, Elsevier

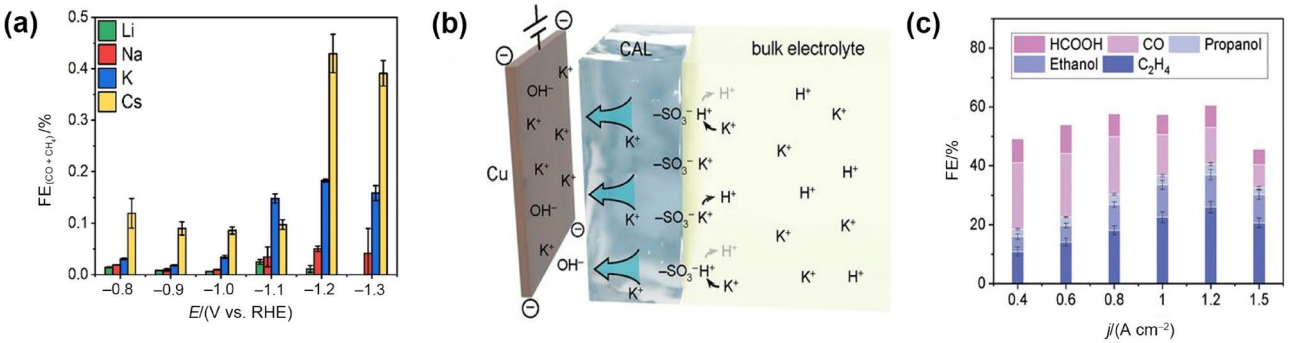

Fig. 5 **a** Combined $CO+CH_4$ Faradaic efficiency after doping Nafion^{TM} CEMs with different cations. Reproduced with permission from Ref. [95]. Copyright © 2022, Elsevier. **b** Transport phenomena through the cation exchange layer next to a Cu electrode and **c** the resulting Faradaic efficiency for various products. Reproduced with permission from Ref. [96]. Copyright © 2021, American Association for the Advancement of Science

3.1.3 Product Crossover

A critical component of industry-scaled CO_2RRs with high selectivity levels is the cost of product separation [99]. In particular, the crossover of products through an IEM contaminates the recirculating anolyte, requiring additional separation and regeneration processes [100, 101]. An inherent advantage of the CEM design relative to the AEM

design is that the electroosmotic drag (EOD) of water, which facilitates neutral product crossover, occurs in a direction approaching the cathode; therefore, anolyte contamination is mitigated. This phenomenon is opposite to galvanic systems, such as direct methanol/ethanol fuel cells, where CEMs experience a higher crossover of methanol and ethanol than AEMs; this action occurs mainly due to higher diffusion coefficients and EOD constants of alcohols in CEMs relative to AEMs [91, 102]. Many strategies for reducing methanol and ethanol crossover in direct methanol fuel cells (DMFCs) have been explored; these techniques can greatly inform strategies for reducing product crossover in CO_2RR reactors [103–106]. These strategies include modifying PFSA-based membranes in the formation of a composite with an inorganic material, such as silica or zirconium phosphate [107, 108], or surface functionalization [109]. Abandoning high alcohol-permeable Nafion^{TM} membranes for nonfluorinated polymers, such as sulfonated polystyrenes, polyether ether ketones, polyimides and polyphenylenes, has been greatly explored [91]. At the cathode of CEM-based CO_2 electrolyzers, due to the low pH, acidic products, such as acetic acid or formic acid, are not typically considered to deprotonate into anionic species and are therefore likely to crossover as neutrally charged species through diffusion. Thus, similar challenges to the development of CEMs for DMFCs are expected. However, in systems with high-pH buffer solutions at the cathodes, anionic product crossover through CEMs may occur. This phenomenon is less likely to occur than it is with AEM systems due to the electrostatic repulsion from the negatively charged functional groups. The crossover rate is mediated by several factors, including the membrane thickness, water content, and operational conditions affecting water uptake, including humidity and temperature [110]. However, an effective mitigation strategy for some products involves simultaneously maintaining a high-pH environment at the cathode and increasing the charge densities in the CEM to maximize the electrostatic repulsion characteristics of products in their deprotonated form.

3.1.4 CEM Stability

The stability of IEMs has been investigated in water electrolyzers as it is being examined at a commercial level, where the devices are reported to operate for long periods (60 000–80 000 h for PEM water electrolyzers and 30 000 h for AEM water electrolyzers) [111]. CO_2 electrolyzers are at a lower technology readiness level than water electrolyzers; therefore, their long-term stability is not a major focus of study. In membrane-based CO_2RR reactors, performance instability is usually diagnosed by a gradual reduction in product selectivity (FE decay) and increased cell voltage (EE decay) [112]. While long-term stability is a complex function of multiple device components and respective decay mechanisms, failures caused by decaying membrane performance can be considered normal contributors, affecting the overall cell resistance and efficiency. Membrane degradation over time impacts various properties, such as water uptake, ionic conductivity, and current-dependent counterion and coion transport, which all impact the performance of the MEA and lead to device instability.

The chemical degradation of membranes is a well-known failure mechanism in PEM water electrolyzers and fuel cells [113, 114]. In water electrolyzers, CEMs are generally vulnerable to the presence of residual O_2 in the cathode of the PEM reactor (the H_2 side), where the reactions between H_2 and O_2 catalyzed by the Pt electrocatalyst accelerate CEM degradation [115, 116]. These reactions generate small concentrations of hydrogen peroxide and very reactive species, such as hydroxyl (HO) and peroxyl (HO_2) radicals. Attacks by radicals on the CEM cause chain scission of the base polymer, reducing the molecular weight of the polymer and the ion exchange capacity (IEC), conductivity, and thickness of the membrane. Note that while radical-mediated degradation pathways have been established in PEM water electrolyzers and fuel cells, studies specific to CEM-based CO_2 electrolyzers have not been reported to date. Several approaches have been used in PEM water electrolyzers to reduce membrane degradation, including treating membranes with ethylenediamine tetraacetic acid (EDTA) to remove various impurities, such as Fe^{2+} (which is a known catalyst of peroxides to form peroxyl and hydroxyl radicals) [117]; this action imbibes membranes with water-insoluble peroxyl inhibitors and radical scavengers [118], developing CEMs with much lower gas crossover characteristics [119].

A strategy for mitigating gas crossover involves using hydrocarbon-based PEMs instead of PFSA CEMs since they typically exhibit lower gas crossover characteristics, reducing CEM degradation by radical attack during proton exchange membrane fuel cell (PEMFC) operations [120]. A drawback of using hydrocarbon PEMs is that their chemical stability against free radical attack is lower than that of PFSAs [121]. To circumvent this issue, sulfonated polyphenylenes consisting entirely of sp^2-aromatic carbon have been developed, that have garnered increasing interest in the fuel cell and water electrolysis domains, but their application in CO_2RR reactors has yet to be reported. As mentioned in Sect. 3.1.1, many hydrocarbon-based PEMs do not exhibit the same phase separation as PFSA-based ionomer materials; therefore, higher IECs are required to obtain high ionic conductivities. This phenomenon results in another challenge for incorporating hydrocarbon PEMs, in which a high IEC increases the water uptake and dimensional swelling, thus increasing the propensity for mechanical degradation in electrolyzers [122].

3.1.5 CEM Summary

CEMs offer high conductivities that reduce the ohmic losses associated with membranes in CO_2RR reactors. However, recently available CEMs suffer from excessive swelling, some crossover of neutral products, such as alcohols, and tendencies to promote acidic cathodic reaction environments; these phenomena increase the rates of HER. The development of CEMs with reduced crossover characteristics of neutral products, in tandem with cell designs that allow the adjustment of the pH of the catholyte, is the main step toward designing efficient CEM-based CO_2 electrolyzers. This design can be tuned by surface modification [123], polymer crosslinking [124], or using an inert reinforcement material to reduce the swelling and water uptake [125]. These actions are design methodologies that must be explored as they reduce product crossover while maintaining high ion conductivity.

3.2 AEMs

As discussed in Sect. 3.1, a major disadvantage of CEMs is their promotion of acidic reaction environments at the cathodes, increasing rates of parasitic HER. To ensure favorable alkaline environments for selective CO_2RRs, AEMs are alternatively used to transport OH^- ions from the cathode to the anode, as shown in Fig. 6. The high pH environment produced at the anode has the added advantages of allowing the use of nonnoble metal OER catalysts (as opposed to IrO_2) and inexpensive flow field plates and gas diffusion media (e.g., stainless steel or Ni instead of Ti) [126].

AEMs have been used in batch-type reactors (H-cells) [76, 127, 128], but they are most frequently studied in flow reactors fed with alkaline anolytes (Fig. 6a); in these reactors, high product selectivity has been obtained (see Table 1). Many advancements have been reported using the hybrid reactor depicted in Fig. 6b, wherein the pH levels of the catholyte and local environment can be precisely controlled to favor specific CO_2RR products [29, 129–131]. Despite this phenomena, AEM-based electrolyzers are plagued with more instability issues than their CEM counterparts; the most prominent problem is the crossover of anionic species [101, 132]. One particular issue is that of CO_2 pumping, whereby the rapid reaction of CO_2 with OH^- to carbonate ions at the cathode and the subsequent crossover to the anolyte significantly reduces the utilization of CO_2. Where KOH is used as the anolyte, the CO_2 pumping reduces the anolyte pH [133–135] and thus reduces cell efficiency due to the increased anodic overpotentials and ohmic losses. To minimize these effects, anolyte solutions must be refreshed regularly [136, 137]. Additionally, a buildup of carbonate ions at the cathode can lead to carbonate salt precipitation, potentially causing rapid cell failure [138, 139].

Nevertheless, AEM-based CO_2RR reactors exhibit higher efficiency and selectivity values than cationic membranes. The development of specialty AEMs for the CO_2RR has been pioneered by Verma and coworkers, who have exclusively studied their impacts on gaseous CO_2 reduction

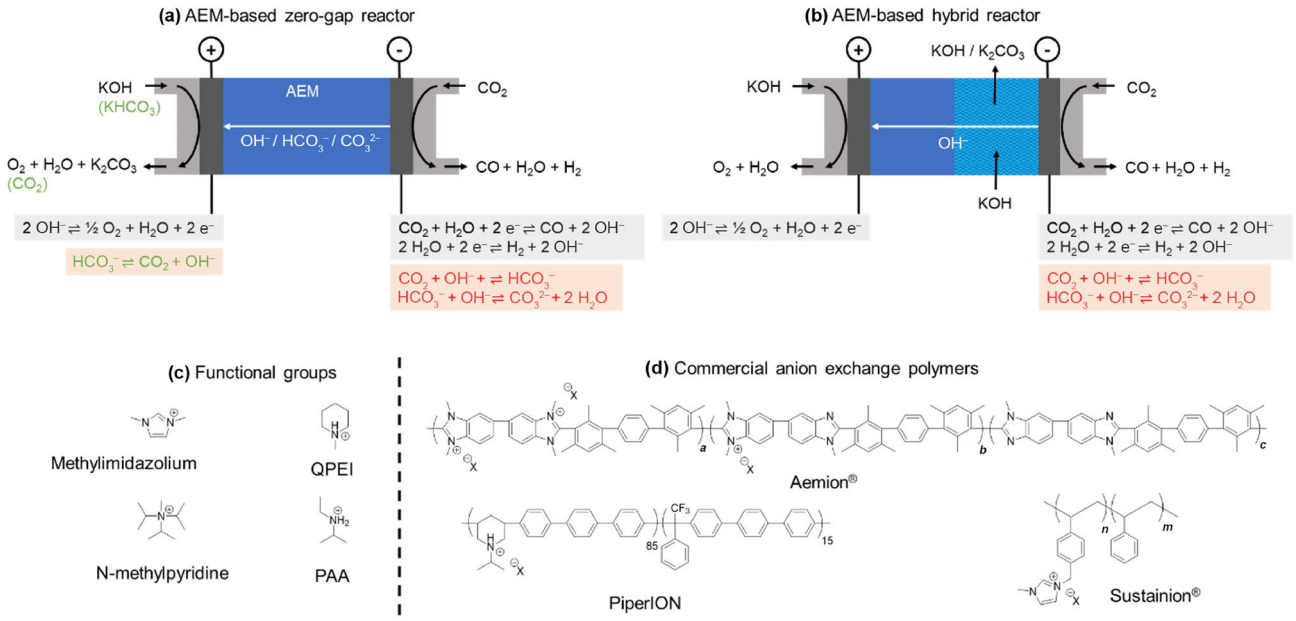

Fig. 6 Designs for AEM-based CO_2 electrolyzers based on **a** zero-gap and **b** hybrid configurations. The carbonation reactions are shown in red. For (**a**), the green reactions indicate the process of CO_2 evolution at the anode when nearly pH-neutral anolytes are used. **c** Common cationic functional groups and **d** some AEM structures used in CO_2RR reactors

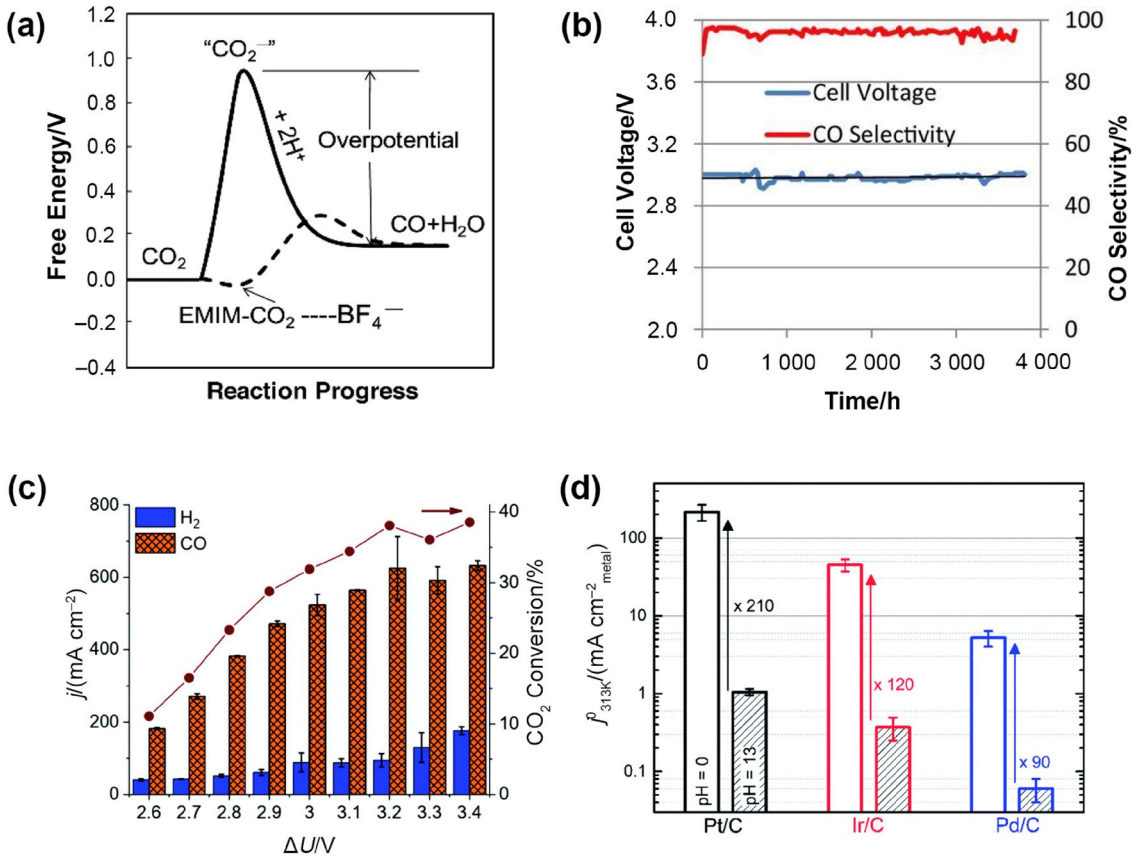

Fig. 7 **a** Activation of the CO_2RR toward CO via an ionic liquid complex. Reproduced with permission from Ref. [145]. Copyright © 2011, American Association for the Advancement of Science. **b** High stability of a CO_2 electrolyzer utilizing a Sustainion® membrane at 200 mA cm^{-2}. Reproduced with permission from Ref. [158]. Copyright © 2018, The Electrochemical Society. **c** Efficient CO_2RR using a PiperION membrane. Reproduced with permission from Ref. [46]. Copyright © 2020, Royal Society of Chemistry. **d** Exchange current density for the HER on carbon-supported noble metal catalysts under acidic and alkaline conditions. Reproduced with permission from Ref. [159]. Copyright © 2014, Royal Society of Chemistry

processes [140, 141]. The extent of the HER and selectivity levels of multicarbon products in zero-gap CO_2 electrolyzers have been explored by using various composite membranes possessing sterically hindered amine groups. The results illustrate that hydrophobic AEMs consisting of highly hindered amine groups [e.g., quaternized polyethyleneimine (QPEI)] impede the access of water molecules to the reaction interface, diminishing HER and increasing C_2H_6 production. In contrast, CH_4 is observed to be the main product when AEMs with few hindered amine groups [e.g., poly-N-isopropylallylamine (PAA)] are attached (Fig. 6c).

Integrating cationic functional groups capable of regulating the CO_2RR environment into chemically stable polymer backbones is a design feature of AEMs. One prominent example is the imidazolium-functionalized styrene membrane developed by Masel et al. [37]. These membranes (commercialized under the name of Sustainion®) show promising functionality in CO_2RRs due to the incorporation of imidazolium groups into AEM structures. The cocatalytic effects of imidazolium ions on CO_2RRs have been proposed by some researchers [142–144] and are allegedly related to the stabilization of the CO_2^- intermediate by the imidazolium ion when the CO_2RR is performed in an ionic liquid electrolyte (Fig. 7a) [145, 146]. These effects are seen for various ionic liquids, including 1-ethyl-3-methylimidazolium (EMIM), 1-butyl-3-methylimidazolium (BMIM), 1-propyl-3-methylimidazolium (PMIM), and 1-butyl-1-methylpyrrolidinium (Bmpyrr) salts [147]. Polystyrene methylimidazolium (PSMIM)-based AEMs (Sustainion®) are reported to exhibit operational stability during CO_2RRs under high current densities (3 000 h with CO selectivity of 95% at 200 mA cm^{-2} and room temperature, Fig. 7b) [148].

Piperidine-based AEMs are another class of alkaline membranes used successfully for CO_2RRs (Fig. 6d). Yin et al. have employed a poly(*N*-methyl-piperidine-co-terphenyl) (QAPPT) AEM in a gas-fed CO_2 electrolyzer delivering industrial-scale current densities, e.g., 500 mA cm^{-2}, with an overall cell voltage of 3 V at 60 °C

and stability of 100 h when operated continuously at 100 mA cm^{-2} and 50 °C [149]. More recently, Endrődi et al. have reported a poly(aryl piperidine)-based AEM (PiperION) with high carbonate conductance for applications in CO_2RRs [46]. A 15-μm thick, PTFE-reinforced PiperION membrane is used in a zero-gap reactor fed with CsOH and CO_2(g) at the anode and cathode, respectively. This device can achieve a maximum CO formation partial current density of ~630 mA cm^{-2} (at 3.2 V) and a full-cell energetic efficiency of 40%, exceeding the results of all previous studies with zero-gap electrolyzers (Fig. 7c). The mechanical stability of PiperION is comparable to that of a commercial AEMs (Sustainion®), allowing the use of thin membranes (as thin as 15 μm) with high carbonate ion conductance.

Several commercial AEM brands have been employed in CO_2RRs, such as Selemion™ (Asahi Glass Co., Japan), which has been used for a wide variety of applications prior to its emergence into CO_2RRs. Several considerations must be considered with Selemion™ membranes, including their low stability in highly alkaline media (> 1 M KOH) [150] and their alcohol diffusive permeability (methanol > ethanol > *n*-propanol) [151]. Moreover, the potential-dependent transport of ionic products of the CO_2RRs, e.g., formate and acetate ions, are prevalent for Selemion™ AMV membranes during the electrolysis of CO_2-saturated $KHCO_3$ solutions at different constant potentials [152].

Polysulfone-based Fumasep® FAA (by Fumatech, Germany) AEMs have been used in CO_2RR reactors. FAA membranes can operate at higher temperatures (up to 60 °C) than Selemion™, and they are reportedly more stable under alkaline conditions [153]. One consideration regarding the Fumasep® FAA membrane is that unlike HCO_3^- and CO_3^{2-} conductivities, the OH^- conductivity is highly dependent on the relative humidity (RH). At 90% RH, the OH^- conductivity is almost 5 times higher than the HCO_3^- and CO_3^{2-} conductivities; at 50% RH, the OH^- conductivity is only 1.3 times higher than the other conductivities, implying that reduced hydration decreases the OH^- conductivity disproportionately [154]. Neosepta™ AHA or AMX (Astom, Japan) and Aemion™ (Ionomr, Canada) membranes are other examples of commercially available AEMs that have been used for CO_2RRs (Table 1). Sustainion® AEMs have been used repeatedly for alkaline CO_2RRs with high current densities [155–157]; however, they appear to be unstable when in prolonged contact with alcohol products. Gabardo et al. have replaced Sustainion® membranes with Aemion™ in the MEA of flow reactors with humidified CO_2 and aqueous $KHCO_3$ (as cathodic and anodic feeds, respectively), after observing that the Sustainion® membranes degrade in the presence of high concentrations of the produced ethanol. With an Aemion™ membrane, the authors can obtain concentrations of ethanol (0.85 M) and *n*-propanol (0.2 M) at an operating temperature of 40 °C [68]. By considering these developments, the key properties of AEMs used in CO_2RR reactors are discussed in the following sections.

3.2.1 CO_2RR Selectivity Under High pH Conditions

The most significant advantage of AEMs over CEMs is the high pH at the cathode. With a similar reduction potential to many of the CO_2RR products, the simplicity of the reaction mechanism, and the absence of mass transport limitations associated with CO_2, HER is a major competing reaction reducing the FEs and thus the EEs of CO_2RR reactors. Therefore, while many CO_2RR catalysts exhibit enhanced CO_2RR activities relative to the HER [160, 161], further suppression is greatly beneficial. This suppression is primarily achieved by considering the pH dependencies of electrochemical reactions, describing changes in the exchange current density and thus the activation overpotential under different pH conditions. The hydrogen oxidation reaction (HOR) and HER proceed much slower under alkaline conditions than under acidic conditions (Fig. 7d) [159, 162, 163]; while an issue for efficient alkaline water electrolysis, CO_2 electrolyzers under alkaline conditions typically experience much higher FEs than CEM-based reactors.

Additionally, the various mechanisms of CO_2RRs exhibit pH dependencies. In early works, Hori has noted that C_2H_4 favorably forms in low concentrations of HCO_3^- electrolytes, whereas CH_4 preferentially forms at higher concentrations due to differences in the local OH^- concentrations (higher with lower [HCO_3^-]) [16, 164]. The enhancement of C_2 product formation at high pH levels is also supported by microkinetic modeling [129]. From the perspective of IEM development, the question remains as to whether AEM design can influence the local concentration of OH^- and thus the selectivity of the CO_2RR. For example, Kim et al. have recently examined a Nafion™ cation exchange layer (CEL), an anion exchange layer (AEL) and a combination of both on sputtered Cu electrodes. The researchers have suggested that the use of a CEL can inhibit OH^- transport and increase the local pH at the electrode surface and thus enhance the selectivity toward C_2 products [165]. The properties of the ion exchange material used in the catalyst layer clearly produce differences in product selectivity and require more comprehensive studies. Specific to membranes in this review, it is concluded that AEM-based CO_2RR reactors typically exhibit higher FEs than CEM-based reactors by better accommodating high pH environments at the cathode.

3.2.2 Rapid Carbonation Reactions

Despite the benefits of high pH levels for suppressing the HER and increasing the selectivity of CO_2RR, the rapid homogeneous reaction of CO_2 with OH^- leads to the carbonation of the AEM, replacing OH^- with HCO_3^-/CO_3^{2-} according to the following reactions.

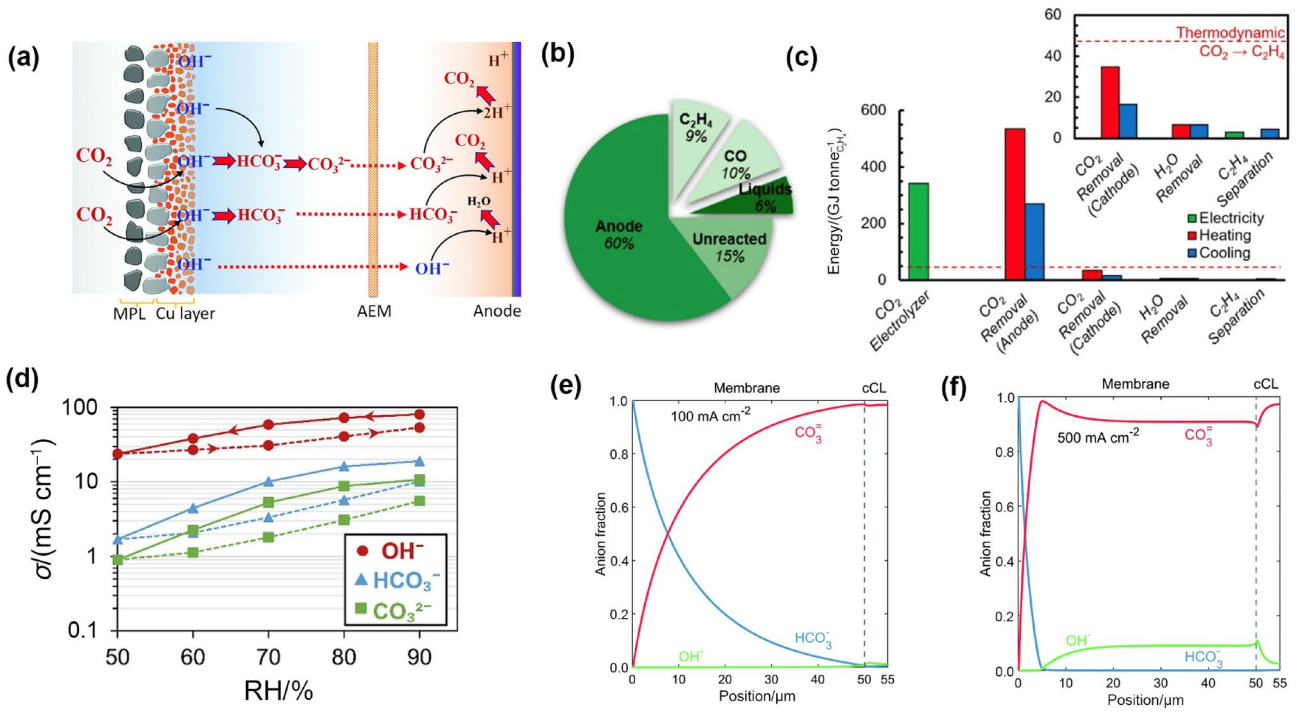

Fig. 8 **a** Carbon balance in a CO_2RR flow reactor using a $KHCO_3$ electrolyte and an AEM. Reproduced with permission from Ref. [133]. Copyright © 2020, Royal Society of Chemistry. **b** CO_2 pathways and **c** energy intensities of CO_2 electrolysis and downstream separation. Reproduced with permission from Ref. [99]. Copyright © 2021, American Chemical Society. **d** Through-plane conductivity of methylated poly(hexamethyl-*p*-terphenyl benzimidazolium) (HMT–PMBI) (Aemion^{TM}) at different relative humidities with different counterions. Reproduced with permission from Ref. [154]. Copyright © 2019, Elsevier. Theoretical anion composition through an AEM at **e** 100 mA cm^{-2} and **f** 500 mA cm^{-2}. Reproduced with permission from Ref. [89]. Copyright © 2019, Royal Society of Chemistry

$$CO_2 + OH^- \rightleftharpoons HCO_3^- \quad \text{(Reaction 1)}$$

$$HCO_3^- + OH^- \rightleftharpoons CO_3^{2-} + H_2O \quad \text{(Reaction 2)}$$

These ions readily crossover the membrane to the anode side by electromigration. Coupled with the OER, these ions can be converted to CO_2 according to Reactions (3) and (4).

$$CO_3^{2-} \rightleftharpoons 1/2O_2 + 2e^- + CO_2 \quad \text{(Reaction 3)}$$

$$2HCO_3^- \rightleftharpoons 1/2O_2 + 2e^- + 2CO_2 + H_2O \quad \text{(Reaction 4)}$$

While trace amounts of CO_2 are often found in the anode due to the diffusional crossover of gaseous CO_2 across AEMs, considerable CO_2 evolution at the anode indicates the electromigration of HCO_3^- and CO_3^{2-} through the membrane (Fig. 8a) [133, 166]. This unwanted transport of HCO_3^-/CO_3^{2-} ions from the cathode to the anode results in the loss of carbon-based reactants from the cathode, consequently reducing the total carbon utilization efficiency [96, 167]. Schmidt and their team found that a typical AEM (Fumasep® FAA 30) pumps up to two CO_2 molecules in the form of crossed-over HCO_3^-/CO_3^{2-} ions to the anode per molecule of CO_2 reduced at the cathode [167]. This phenomenon equates to CO_2/O_2 ratios in the anode of 4, 2 and 0 when the charge carriers are 100% HCO_3^-, CO_3^{2-} and OH^-, respectively. Theoretically, the carbonation of the AEM can lead to 50% and 75% losses in the available carbon for two- and six-electron CO_2 conversion reactions, respectively [96]. This reduction in CO_2 utilization efficiency can be very detrimental to the economic viability of AEM-based CO_2RR reactors. Recently, it has been shown that separation of CO_2 from the anode gas has a higher energy demand than the electrolyzer (Fig. 8b, c) [99]; thus, mitigation strategies are needed. One such strategy might simply involve developing systems that can operate at high enough current densities so that the rate of OH^- migration through the AEM exceeds the rate of conversion to CO_3^{2-}; however, modeling suggests that current densities must be > 1 A cm^{-2} for OH^- to become the dominant charge carrier [89].

Another deleterious effect of AEM carbonation is the neutralization of the anolyte. The transport of HCO_3^-/CO_3^{2-} ions to the anode in AEM-based electrolyzers with highly alkaline KOH anolytes reduces the pH of the anolyte, consequently shifting the OER potential in the positive direction [135, 168]. Additionally, the uptake of (bi)carbonate ions by the AEM impacts the overall

conductivity of the membrane due to them exhibiting larger sizes and lower mobilities than OH^-. These two phenomena increase the overall cell voltage and thus lead to considerable energy losses. Therefore, to enable stable operation, KOH anolytes must be regenerated in a caustic recovery loop [169]. This process is even more energy -intensive than the separation of CO_2 from anode gases [170]; unless greatly reduced, alternative reactor configurations that avoid this process are typically favored.

3.2.3 Ionic Conductivity

Due to the typically lower diffusion rates of OH^- relative to H^+ (diffusion coefficient, $D_{OH^-} = 5.27 \times 10^{-5}$ cm^2 s^{-1}, $D_{H^+} = 9.31 \times 10^{-5}$ cm^2 s^{-1}) [171], the conductivities of AEMs in their OH^- form experience disadvantages with respect to CEMs in the H^+ form [154, 172]. The replenishment of OH^- ions with CO_3^{2-} ($D = 9.23 \times 10^{-6}$ cm^2 s^{-1}) or HCO_3^- ($D = 1.18 \times 10^{-5}$ cm^2 s^{-1}) [171] reduces the ionic conductivity of an AEM even further (Fig. 8d), leading to a higher cell resistance and a lower EE. AEM carbonation makes hydroxide conductivity measurements challenging since controlled atmospheric environments are required to avoid the diffusion of atmospheric CO_2 into the AEM. Ziv and Dekel have demonstrated a method for measuring the true value of the hydroxide conductivity of AEMs in which the cathodic in situ formation of OH^- flushes the HCO_3^-/CO_3^{2-} ions inside the AEM out to the anode where they are released as CO_2 [173]. The decarbonation of the membrane is conducted until all the HCO_3^- ions in the membrane are replaced with OH^- [174]. At this stage, the anion conductivity of an AEM is recorded as a function of time until a plateau value indicating the true OH^- conductivity is reached. This method provides reproducible and accurate OH^- conductivities that can be used for characterization purposes. From a practical standpoint, in a CO_2 electrolyzer with high concentrations of CO_2 fed to the cathode, the hydroxide conductivity may not be as relevant as in water electrolyzers or alkaline fuel cells since it is believed that the main charge carriers in the membrane are HCO_3^-/CO_3^{2-} ions (Fig. 8e, f). However, knowing the real hydroxide conductivity, especially as a function of relative humidity, is a useful comparative metric for AEMs where hydroxide is ultimately the charge carrier of choice [46]. In lieu of AEMs that retain high OH^- conductivities during CO_2RRs, other strategies for reducing the overall ohmic resistance of the collective MEA have been explored for other electrochemical energy conversion devices. For example, an alternative MEA design strategy based on the direct deposition of the catalyst on the membrane reduces the ohmic resistance by improving the contact of the ion conducting channels in the catalyst layer and membrane [175–177]. Adopting these techniques is becoming increasingly important for CO_2 electrolyzers as the achievable current densities increase.

3.2.4 Product Crossover

In addition to the crossover of the reactants (e.g., carbonate ion crossover), product crossover can occur, which may reduce the FEs unless the transported products are retrieved from the anolyte solution. The crossover of ionic products in CO_2 electrolyzers across commercial AEMs, such as Fumasep® [167], Selemion™ [152], Neosepta™ [178], and Sustainion® [179, 180], have been reported [26, 180]. Negatively charged products, such as formate ($HCOO^-$) and acetate (CH_3COO^-), begin to migrate through the AEM, especially at high current density values when the HCO_3^-/CO_3^{2-} charge carriers in the membrane deplete. In this case, the transport of formate, acetate, OH^-, HCO_3^- and CO_3^{2-} is required to maintain device electroneutrality [39]. Anion crossover is found in various CEMs, such as Nafion™, although the negatively charged functional groups indicate that crossover is generally mediated by diffusion; hence, the crossover rate is affected by the membrane thickness, water content, and operational conditions, including humidity and temperature [110]. Due to electrostatic repulsion by the negatively charged functional groups, anionic product crossover through CEMs is typically much less than that of AEMs and is a leading motivator for BPMs where CELs reduce the crossover of anionic species [178].

3.2.5 System Stability

When CO_2RR reactors are fed with KOH or NaOH solutions, the chemical stability of AEM is compromised the nucleophilic attack of OH^- on either the immobilized ion exchange functional groups or the backbone of the polymer. OH^- attack can lead to the loss of functional groups and a reduction in WU and ion exchange capacity (IEC) of the AEM; which, in turn, reduce the hydroxide conductivity. OH^- attack on the polymer backbone weakens the tensile strength and mechanical stability of the membrane; these weakened properties are often used as indirect evidence of the degradation of the polymer backbone as opposed to the losses of ionic functional groups.

The resistance of an AEM to OH^- nucleophilic attack can be tuned by modifying the chemical structure of the constituent polymer. Generally, reduced alkaline stability is observed for AEMs bearing electrophilic functional groups that are less sterically protected. For instance, AEMs with quaternary ammonium (QA) groups and beta hydrogen are

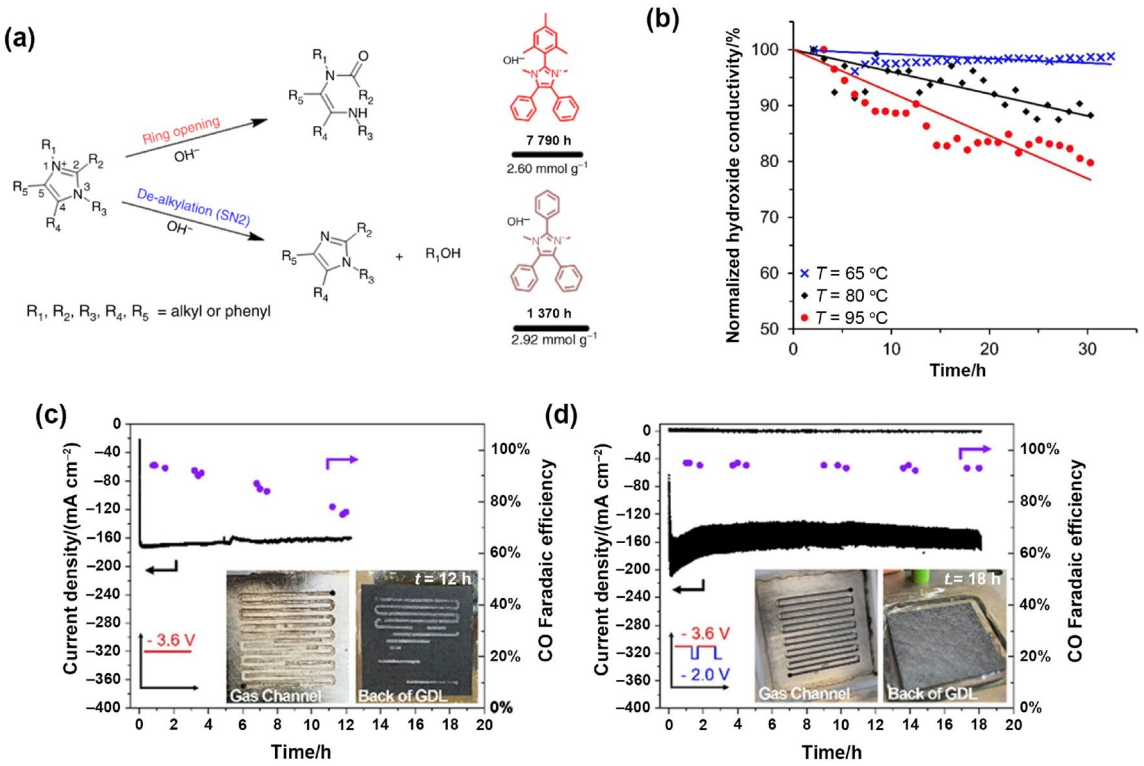

Fig. 9 **a** Degradation pathways of an imidazolium cation alongside the differences in half-life values for a C2 protected (top) and unprotected (bottom) imidazolium. Reproduced with permission from Ref. [187]. Copyright © 2019, Springer Nature. **b** Loss of hydroxide conductivity for a low-density polyethylene radiation grafted membrane functionalized with benzyl trimethylammonium (BTMA–LDPE). Reproduced with permission from Ref. [189]. Copyright © 2020, American Chemical Society. Stability of a CO_2 electrolyzer **c** without and **d** with self-cleaning cycles, alongside images showing salt precipitation in the flow field plates. Reproduced with permission from Ref. [193]. Copyright © 2021, American Chemical Society

more susceptible to OH^- nucleophilic attack followed by Hofmann elimination. However, AEMs with cage-like QA functional groups, such as 1,4-diazabicyclo[2.2.2]octane (DABCO) and quinuclidinyl-(1-azoniabicyclo[2.2.2]octane), are more stable than QA due to the rigid cage structure, hindering Hofmann elimination [118].

Polymers exhibit different stabilities with or without attached functional groups. For example, while polysulfone is alkali-resistant alone, the addition of QA functional groups via $–CH_2$-linkages renders the polymer backbone hydrophilic and allows OH^- ions to approach the alkaline-sensitive sulfone groups [181]. Alternatively, the charged functional group is embedded in the polymer backbone to form an ionene. For example, a highly stable benzimidazolium ionene is achieved by steric crowding around the C2 position by replacing the phenyl group in polybenzimidazolium with a mesitylene group [182] and later a hexamethyl-*p*-terphenylene for the purpose of decreasing the water solubilities of membranes [183]. The C2 position of the polybenzimidazolium remains susceptible to nucleophilic addition and ring opening. While steric protection provides significant enhancement, using an inherently stabler imidazolium group provides even greater stabilities [184–186], with half-lives extrapolated to several thousand hours in 3 M NaOH at 80 °C (Fig. 9a) [187]. When discussing the alkaline stability of AEMs, it is critical to acknowledge that the true stability during electrochemical operation depends heavily on its hydration state (Fig. 9b). For example, in the anion exchange membrane fuel cell (AEMFC) research field, a stoichiometric difference of 6 for water at the cathode and anodic reactions results in challenging water management, where the cathode is susceptible to drying out and the ionomer/AEM is more susceptible to degradation at low RH levels [188, 189].

For CO_2RR reactors, excess water can accumulate at the cathode CL when the rate of the water entering the cathode catalyst layer (through the IEM and/or humidification of the CO_2 feedstock) is higher than its consumption rate during electrolysis. This phenomenon is known as cathode flooding; it increases cell voltages (i.e., decreases EEs) and promotes the HER (i.e., decreases selectivity) [60]. In zero-gap reactors that use gaseous cathodic feedstocks, the crossover of anolyte cations (e.g., K^+ when KOH is used) through an AEM results in the precipitation of (bi)carbonate salts on the cathode GDE,

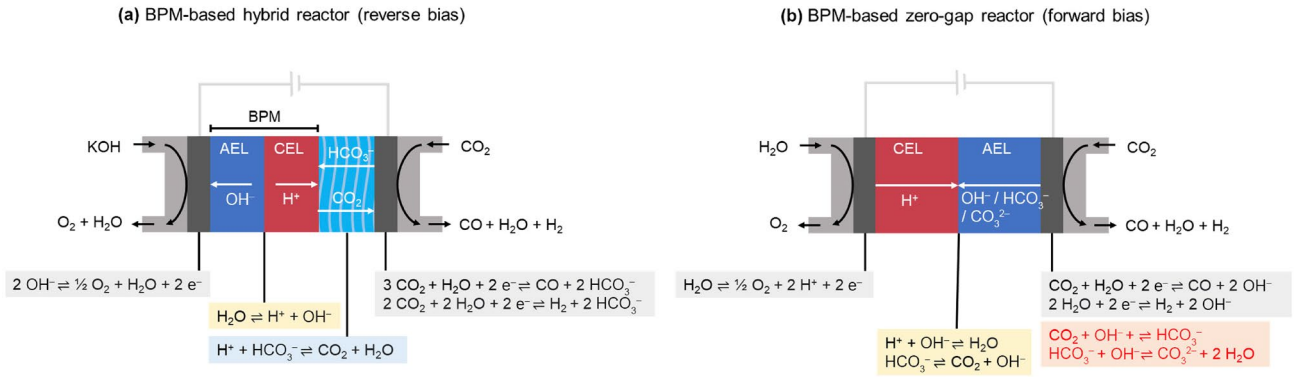

Fig. 10 Designs for CO_2 electrolyzers based on **a** a BPM-based hybrid reactor (reverse bias mode) with liquid feedstock fed to the cathode and **b** a BPM-based zero-gap reactor (forward bias mode)

obstructing the reactant flow and reducing the device stability [190]. Migration of coions (e.g., the transport of K^+ across an AEM) is more likely to occur when high concentrations of anolyte are fed to the anode. When the ionic strength of the aqueous solution in contact with the membrane greatly exceeds the ionic strength of the membrane interior, coion uptake takes place. This phenomenon is amplified by the magnitude of current passing through the cell. In a CO_2 electrolyzer, where the (bi)carbonate ions are the main charge carriers within the IEM, the electromigration of K^+ coions with large transference numbers across the membrane enables the IEM to maintain its ionic conductivity [191]. IEMs with high concentrations of fixed charge groups (i.e., high IEC) usually exhibit lower coion uptake characteristics; however, the effect of IEC can be outweighed by the high-water content in excessively swollen membranes [192].

As a result of these processes, flooding and salt precipitation are often the main contributors to performance decay in gas-fed, zero-gap, AEM-based CO_2 electrolyzers, especially at high current densities (> 200 mA cm^{-2}). However, both undesirable processes can be mitigated by tuning the membrane properties. For example, a study by Reyes et al. shows that using thin, high WU AEMs [60] can attenuate flooding and salt precipitation in reactors that use humidified CO_2 streams as the feedstock. Authors showed that humidification reduced the amount of water required through the AEM, and an increased water permeation enhanced the back convection of excess water [190].

3.2.6 AEM Summary

Research on AEMs in recent decades, as encouraged by the research advancements of AEMFCs [194], has led to a selection of commercialized AEM materials exhibiting ion conductivities equal to those of CEMs. With high pH values at the cathode, CO_2RR reactors utilizing AEMs typically exhibit a higher initial FEs through the suppression of the HER; from this perspective, CO_2RR reactors are promising candidates for achieving the EEs required for industrial systems. However, stability issues derived from nucleophilic OH^- ion attack and higher product and carbonate ion crossovers are inherent to the positively charged functional groups of the IEM. Novel AEM designs are required to address these issues, such as surface functionalization or crosslinking, to reduce product crossover [60]. System parametrization that can accommodate novel AEMs is required since water uptake and ion transport efficiency are inextricably linked [195]. Alternatively, some of the issues associated with AEMs might be circumvented altogether. For example, carbonation reactions can be avoided by considering only the CO reduction reaction (CORR) to C2 products (as opposed to CO_2RR) in a tandem electrolysis system; considering the improved economic viability, CORR rectors might be the future of reactors incorporating AEMs [170, 196].

3.3 Bipolar Membranes (BPMs)

Another IEM class used in CO_2RRs is the BPM, fabricated by laminating a cation exchange layer (CEL) with an anion exchange layer (AEL). Cation and anion mobile counterions are transported through their respective domains and either combine to form water (forward bias mode, i.e., CEL at the anode) or are transported away from the interface under the influence of an electric field facilitating the dissociation of water (the reverse bias mode, i.e., CEL at the cathode) [55] typically aided by the presence of catalysts at the CEL–AEL interface of the BPM (Fig. 10a) [56, 57].

The reverse bias mode has been explored for water electrolysis systems due to the benefit of coupling facile HER under low pH conditions at the cathode and the possible use of nonnoble metal OER catalysts at the anode (high pH) [197]. For CO_2 electrolysis, the BPM in the reverse bias mode limits the crossover of HCO_3^-/CO_3^{2-} ions, allowing for different pH conditions for the anode (high pH) and the cathode (low pH) compartments to be maintained for a long duration [54, 198]. Despite these benefits of reverse bias BPMs, the

low pH of the cathode under these conditions favors parasitic HER, reducing the FEs of gas-phase CO_2RRs. However, a low pH promotes the protonation of bicarbonate and carbonate species, allowing the use of liquid CO_2 feedstocks in a hybrid-type reactor (Fig. 10a) [58, 71].

Due to the promotion of HER with the cathode facing the CEL in the reverse bias mode, the forward bias mode (Fig. 10b), in which OH^- and H^+ recombine at the interface, has been investigated [94, 199, 200]. This configuration results in the formation of water and CO_2 at the CEL–AEL interface of the BPM, requiring sufficient porosity at the interface near the cathode to allow CO_2 and water to egress; otherwise, the accumulation at the CEL–AEL interface causes the delamination of the two layers [131].

To date, Fumasep® FBM membranes are the only commercially available BPMs that have been used for CO_2RR. However, there are various bipolar membranes that have been traditionally employed in other electrochemical applications, such as electrodialysis and water splitting, that might be potentially suitable for implementation in the CO_2RR [201, 202]. BPMs are fabricated by combining commercially available or custom-made AEMs and CEMs, providing a unique opportunity for tuning the overall properties of the BPM through modifying each layer. For example, a recent work by Yan et al. has shown that the HER significantly decreases in a zero-gap gas-phase CO_2 electrolyzer when the Nafion™ layer of BPM is modified with poly(acrylic acid) (PAA) and poly(allylamine hydrochloride) (PAH) [200]. The layer-by-layer depositions of PAA ($pK_a = 4$–6) and PAH ($pK_a = 8$) on highly acidic Nafion™ ($pK_a < 1$) provide a polymeric buffer layer between the Nafion™ and the catalyst layer, increasing the pH at the cathode and hence reducing the extent of the HER. Other strategies for suppressing the HER by reducing the acidity of the CEL side of the BPM include the incorporation of anionic binding ionomers into the cathodic catalyst layer and adding liquid buffer layers between the membrane and the cathode GDE [203].

BPM fabrication by CEM/AEM lamination is most effective when the individual layers are chemically and physically compatible. For example, the water uptake of the CEL should match the AEL so that suitable and uniform humidification is achieved. If the membranes are not compatible, the performance of the BPM degrades, and problematic issues, such as water accumulation and decreased mechanical stability of the BPM interface, appear [204]. To minimize such issues, Chen et al. have designed novel electrospun 3D BPMs (Nafion™ CEL–junction–AEL) for potential applications in high-current–density CO_2 electrolyzers [205]. The enhanced mechanical integrity of the 3D BPM originates from the coelectrospun junction consisting of water dissociating catalyst sprayed between the fibers during the concurrent electrospinning of CEL and AEL fibers. The high catalyst loadings obtained with this method, combined with the entanglement of the fibers with opposite fixed charges, facilitate the migration of water dissociation products away from the junction. The intertwined structures of the fibers throughout the membrane improve the mechanical stability, especially at high current densities, suggesting potential applicability for CO_2RRs.

In addition to considering the mechanical properties of the BPM, the overpotential imposed on devices by the sluggish kinetics of water dissociation at the CEL–AEL interface is substantial even at low current densities (i.e., > 100 mV at 20 mA cm^{-2}). Therefore, to obtain a BPM that can support industrially relevant currents (> 100 mA cm^{-2}) at a reasonable cell voltage, suitable water dissociation catalysts must be employed at the CEL–AEL interface. Polymer-based catalysts [206] or metal hydroxide catalysts, such as $Fe(OH)_3$ [207], and graphene oxide [208], have been used to accelerate the water dissociation reaction at the interface. One strategy for further reducing the water dissociation overpotential involves applying a bilayer catalyst structure (e.g., IrO_2 at CEL and NiO at the AEL side) to match the local pH of the water dissociation on each side of the bipolar interface [56].

The BPM is an emerging IEM design for CO_2RR reactors, although implementation requires the careful consideration of the low cathode pH and water dissociation overpotential in reverse bias, in addition to the evolution of CO_2 and water formation at the CEL–AEL interface during forward bias operation. Nonetheless, while BPM development remains relatively new, some properties governing the efficiencies of CO_2RR reactors have emerged, as discussed in the proceeding sections.

3.3.1 Overpotentials for Water Dissociation

In BPM electrochemical devices, the ionic conductivities of oppositely charged ions are permitted by either the continuous generation of H^+ and OH^- ions or the recombination to H_2O at the CEL–AEL interface. In configurations where the AEL side of the bipolar membrane faces the anode and the CEL side faces the cathode (i.e., reverse bias), sufficient ionic transport is maintained by water dissociation to OH^- and H^+ at the CEL–AEL interface. The dissociation of water occurs through an electric field-enhanced mechanism, known as the second Wien effect, due to a potential field developing across the CEL–AEL interface [209]. The resulting protons are transported across the CEL to the cathode, while the hydroxide ions are transported across the AEL to the anode (Fig. 11a) [72].

The ion concentration profiles and transport mechanisms in the BPM are typically studied in a 4-electrode H-cell where two reference electrodes adjacent to the AEL and CEL allow for the measurement of the membrane potential. Polarization curves recorded with pH-neutral electrolytes, as shown in Fig. 11b, typically include a limiting current density at membrane potentials < 0.83 V, which predominantly corresponds to electroneutrality being maintained by coion leakage through the BPM (e.g., cations passing through the

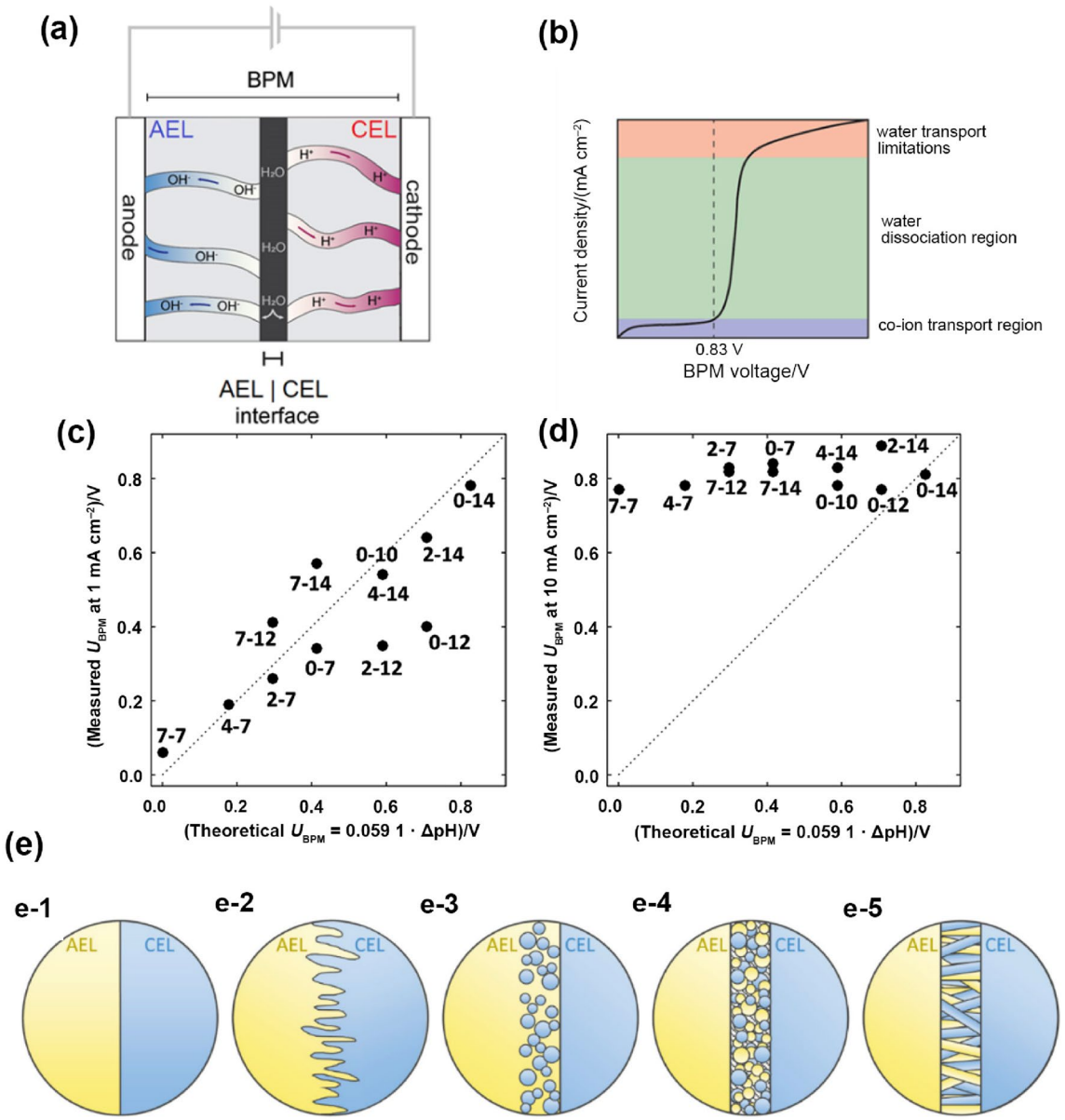

Fig. 11 **a** Diagram of a bipolar membrane under a reverse bias electric field. OH^- and H^+ ions generated from water dissociation at the CEL–AEL interface migrate to the anode and cathode, respectively, maintaining a high pH at the anode and a low pH at the cathode. **b** Typical polarization curve featuring the current–potential characteristics of a BPM operating under reverse bias in near pH-neutral electrolytes. Adapted with permission from Ref. [55]. Copyright © 2021, Elsevier. Measured versus thermodynamic membrane potential (U_{BPM}) for BPM under reverse bias at **c** low current density (1 mA cm^{-2}) and **d** high current density (10 mA cm^{-2}). Reproduced with permission from Ref. [210]. Copyright © 2018, Royal Society of Chemistry. The numbers indicate the pH in the catholyte–anolyte. **e** Schematic diagrams of different methods for extending the bipolar interface: e-1, smooth; e-2, grooved; e-3, heterogeneous; e-4, heterogeneous; and e-5, electrospun junctions. Reproduced with permission from Ref. [55]. Copyright © 2021, Elsevier

AEL and anions passing through the CEL). A high concentration of coions in electrolytes results in an increase in coion leakage by overcoming Donnan exclusion [86, 211]; therefore, a large limiting (plateau) current indicates high coion leakage either due to the poor selectivity of the membrane or the exposure to high concentrations of coions [212]. Nevertheless, the magnitude of the plateau with lower concentration electrolytes allows for the permselectivity of the entire BPM to be evaluated.

This coion transport region is followed by a rapid increase in the current density above the limiting value due to the more significant contribution of water dissociation [212, 213]. The onset of water dissociation at the CEL–AEL interface is governed by the pH difference across the junction

(e.g., 0.83 V for a pH difference of 14). Polarization curves are typically complicated by the inclusion of Donnan potentials in the measurements, indicating that the actual onset of water dissociation; thus, the pH difference at the junction is only determined by different methodologies [214, 215]. Vermaas et al. have shown that when BPMs operate in reverse bias mode at 1 mA cm^{-2}, the membrane potential is lower for smaller ΔpH values and is closer to the expected junction potential for water dissociation calculated from the pH of the bulk electrolytes (deviation below the dotted line is attributed to coion leakage, Fig. 11c) [210]. At a current density of 10 mA cm^{-2}, the voltage of the membrane is almost independent of the pH difference across the BPM (Fig. 11d) and is very near the theoretical voltage required for driving water dissociation at the interface (0.83 V). These findings illustrate that while the pH difference across the BPM interface defines the potential at high current densities, the membrane potential depends on the concentration of the bulk electrolyte at low current densities. When supporting electrolytes are used to ensure a large pH difference between the cathode and anode, the limiting current density for coion leakage is not typically observed since a junction potential of 0.83 V becomes necessary for the current to be passed between the working electrodes (considering 0.40 V vs. the SHE at pH = 14 for the OER at the anode and 0 V vs. the SHE at pH = 0 for the HER at the cathode).

More critical for the initial efficiencies of the CO_2RRs utilizing BPMs are the high overpotentials required for efficient water dissociation; this overpotential is typically > 100 mV at current densities as low as 20 mA cm^{-2} [56]. One method for decreasing the overpotential for water dissociation is to ensure a thin interfacial region that maximizes the electric field required for the second Wien effect. However, decreasing the thickness of the interface results in highly localized dehydration as a side effect. One effective strategy for mitigating dehydration is to increase the interfacial surface area using methods, such as electrospinning CEL and AEL materials into a 3D layer, resulting in significant reductions in water splitting overpotential [216]. Other techniques for increasing the surface area of the interface are discussed in Sect. 3.3.3. The incorporation of metal oxide/hydroxide water dissociation catalysts at the interfacial layer is crucial for obtaining adequately low overpotentials of the junction [217–219]. Recently, it has been found that thorough consideration of the water dissociation catalyst(s) employed with regard to their point of zero charge (PZC), the local pH of the CEL–AEL interfaces, and the stabilities of the catalysts at these pH values are more important than enhancing the electrical field [56]. It is shown that a PZC near that of the local pH is optimal for ensuring both efficient protonation and deprotonation steps required for water dissociation. These findings demonstrate that using two water dissociation catalysts specific for CEL and AEL conditions results in water electrolysis performance of a BPM system comparable to that of an AEM system. It is therefore anticipated that while the recent statuses of commercial BPMs exhibit higher resistance levels to those of AEMs or CEMs, future advances are likely to reduce this gap.

3.3.2 Anionic and Neutral Product Crossover

BPM-based CO_2RR reactors are primarily used to mitigate the crossovers of anionic and neutral products. In reverse bias mode, the presence of a CEL at the cathode greatly limits the crossover of anionic species, such as formate and acetate, through the Donnan exclusion principle [178]. Concentrations of accumulated anionic species in the cathode that exceed that of the fixed ion concentration of the CEL might incur significant diffusion to the AEL and subsequent migration to the anode. This effect should be considered when determining operational parameters for an industrial system, such as the cell temperature, operating current density, reactant flow rates and reactor design, since they greatly influence the accumulation of products at the cathode. Carbonate ion crossover decreases with the CEL facing the cathode, where the ready protonation of a liquid HCO_3^-/CO_3^{2-} feed to gaseous CO_2, which subsequently reduces at the cathode, complements the more efficient CO_2 capture [220]. When used in reverse bias, BPMs reduce the crossover of neutral products relative to AEMs; the continuous outward fluxes of protons toward the cathode result in the electroosmotic drag of water opposing the diffusion direction [178, 221].

For BPMs in forward bias, the protonation of leaked HCO_3^-/CO_3^{2-} to CO_2 at the interface prior to their migration across the AEL greatly inhibits the final carbon crossover to the anode side [131, 167, 222]. However, as discussed in the next section, the formation of water and CO_2 at the interface can result in BPM blistering in forward bias unless sufficient removal toward the cathode outlet is ensured. The inward flux for forward bias BPMs and subsequent electroosmotic drag might lead to a buildup of neutral products at the CEL–AEL interface, although this has not yet been reported for CO_2RR.

3.3.3 Mechanical Degradation of BPMs

The stability of a BPM is defined by the stability of the polymer layers and the structure of the bipolar interface [55]. As discussed previously in Sect. 3.1.4 and Sect. 3.2.5, the chemical stability of the CEL is less of a concern when in contact with neutral electrolyte solutions, such as those used in CEM-based CO_2RR reactors; however, the AEM layer may experience degradation under alkaline conditions. In addition to chemical stability, CEL and AEL should demonstrate good mechanical stability. Mechanical degradation is usually caused by local stressors, leading to early life failures, especially for thin membranes. Internal stress arises from changes in the temperature and humidity during operation, nonuniform

cell assembly pressure, assembly displacement, gas pressure difference, and membrane defects; these stress factors are all potential contributors to the loss of mechanical integrity in the membrane [223]. Differences in the properties of the CEL and AEL of a BPM, such as swelling properties, can lead to layer delamination [224]. Delamination is exacerbated under forward bias operation where the irreversible buildup of water, salts and CO_2 can result in the delamination or mechanical deformation of the BPM [225]. Layer adhesion can be improved by increasing the interfacial surface areas between the layers by roughening the surfaces of the IEMs and developing a BPM from a single material to provide mechanically similar CEL and AEL layers [216]. The most successful recent strategy for mitigating BPM delamination in forward bias involves providing sufficient pathways for both H_2O and CO_2 removal at the cathode, primarily by using an ultrathin AEL at the cathode so that there are sufficient pathways between the CEL–AEL interface and the cathode outlet [131, 167, 222].

A strategy of differential layer thickness has been adopted for BPMs under reverse bias; for high current densities ($\geqslant$100 mA cm^{-2}), the generation rates of H^+ and OH^- are limited by the transport of water molecules into the interface, leading to an increase in the operating voltage and destruction of the membrane by dehydration [208]. Therefore, sufficient water permeation to the interface is critical. For example, Oener et al. [226] have enhanced the water permeation properties for a water electrolysis system by reducing the thickness of the CEL in a reverse bias BPM. With improved water permeation to the interface, an additional consideration of the stability of the water dissociation catalysts is highlighted. This phenomenon is not an issue in the forward bias configuration where water dissociation catalysts are not needed. Additionally, a thin CEL is anticipated to reduce the beneficial mitigation of anionic and neutral product crossover in CO_2RR reactors, as discussed in Sect. 3.2.

A larger surface area of the bipolar interface reduces localized dehydration at the interface resulting from water dissociation and consequently mitigates some of the mechanical degradation issues that result in. This phenomenon has the added benefit of reducing the mass transport overpotential for water transport to the dissociation sites. Several modifications to the smooth bipolar junction similar to Fumasep® FBM (Fig. 11e-1) have been reported to maximize the interface surface area. The roughening of BPM interfaces can be achieved through modifying one layer prior to laminating the second layer of opposite charge, filling the resultant grooves (Fig. 11e-2). Methods for achieving this goal include the use of sandpaper or a roughened template during the manufacturing process of the first ion exchange layer. Another approach involves fabricating heterogeneous interfaces where the resin particles of one ion exchange polymer are entirely surrounded by the matrix (Fig. 11e-3) or polymer particles (Fig. 11e-4) of the second ion exchange layer [227]. In this structure, which is characteristic of BPMs prepared by hot pressing, each layer is in direct, extended contact with the opposite ion exchange polymer. Electrospun heterogeneous interfaces (Fig. 11e-5) can be used, achieving a randomly distributed network of anion and cation polymer nanofibers [216, 228]. In addition to greatly increasing the interfacial area of the BPM, the intertwined fibers from electrospinning provide excellent adhesion at the interface, further improving the resistance to delamination. For example, Powers et al. have reported a low voltage drop of approximately 0.82 V at 1 000 mA cm^{-2} and 60 h stable water splitting operation at 800 mA cm^{-2} for a graphene oxide containing BPM made by electrospinning SPEEK and quaternized poly(phenylene oxide) [229].

3.3.4 BPM Summary

BPMs have received renewed interest in recent years as viable alternatives for AEMs and CEMs in electrolysis devices. For CO_2RR reactors, the primary benefits of BPMs concern the mitigation of the crossovers of both HCO_3^-/CO_3^{2-} species and products, which are detrimental to reactor efficiency and stability. In water electrolyzer systems and under reverse bias conditions, improvements in the understanding of water dissociation at the CEL–AEL interface have led to the performance levels of BPM water electrolyzers being comparable to those of AEM water electrolyzers [56, 230]; however, many of these advancements concerning the CEL–AEL interface are not yet commercialized. Typically, reports on CO_2RR reactors utilizing BPMs in reverse bias exhibit much higher cell voltages and reduced FEs for CO_2RRs due to the CEL facing the cathode, favoring low pH conditions. Nevertheless, the protonation of liquid feedstocks provides a promising avenue for coupling CO_2RR reactors with bicarbonate-saturated CO_2 capture solutions [71, 220]. To ensure a high pH at the cathode, forward bias BPMs have thus received increasing attention, although initial development has been stymied by the delamination of the interface. Recent advancements in BPM and cathode design have helped to address these issues while concurrently maintaining high FE at the cathode [131, 167, 222]. Nevertheless, cell voltages remain higher than those of AEM systems; therefore, the further study and understanding of these voltage losses is needed.

4 Comparison of IEMs

In recent years, the rapid development of CO_2RR reactors has led to a wide variety of device configurations, each with unique challenges for further development. The purpose of this section is to summarize the origins of reactor performance levels with different types of IEMs and present viable targets to expedite future research.

Table 2 Comparison of operational conditions of CO_2 electrolyzers using CEMs, AEMs, and BPMs

IEM	Common type of electrolyzer	Cathode pH condition	Anode pH condition	Cons	Pros
CEM	H-cell	Acidic–neutral	Acidic–neutral	Promotes hydrogen evolution reaction (HER) Limited to low T (< 100 °C) Excessive swelling, especially when high concentrations of alcohols are present Costly	IEM high proton conductivity
	Hybrid flow reactor	Neutral–mild alkaline	Neutral–mild alkaline	Energy losses due to the ohmic resistance of the electrolyte layer	Attenuates HER
AEM	Zero-gap flow reactor	Highly alkaline	Mild–highly alkaline	Electrolyzer instability due to reduction in anolyte pH and salt precipitation at the cathode Crossover of neutral and anionic CO_2RR products	Suppresses HER Allows for use of nonnoble metal OER catalysts
BPM (reverse bias)	Hybrid or zero-gap flow reactor	Mild acidic	Alkaline	Highest E_{cell} Lowest EE Prone to physical damage and delamination	Minimal crossover Independent adjustment of the pH for the anode and the cathode compartments and hence greater selectivity
BPM (forward bias)	Zero-gap flow reactor	Alkaline	Neutral–acidic	BPM degradation by delamination	Minimal crossover

The advantages and disadvantages of using an IEM in a given type of CO_2RR reactor, as discussed in the previous sections, are summarized in Table 2. From this comparison, the trends in the energetic efficiency, CO_2 conversion efficiency and device stability are not completely clear. Direct comparisons are complicated by various parameters, such as the wide range of catalysts employed, the studied CO_2RR products, the supporting electrolyte used, and the cell temperature and pressure. However, a few trends emerge that inform future research and development for each type of IEM.

4.1 Energetic Efficiency

As detailed in the introduction and in Eq. (1), EE is the product of the voltage efficiency (i.e., $\frac{E_i^0}{E_{cell}}$) and the FE. These efficiencies are inclusive of the catalytic overpotentials at the electrodes' or at the BPM interface, the ionic resistance, the pH conditions of cathodic and anodic environments, and the product losses through crossover mechanisms. Reporting on the total EE of a CO_2 electrolyzer cell is rare because many studies are only concerned with the cathodic overpotentials, negating the voltage losses from the membrane and the anode. Additionally, CO_2RR reactors designed for C_{2+} products, such as ethylene, typically exhibit lower FEs due to the competing pathways leading to other similar products, such as ethanol [231]. However, by plotting reported faradaic efficiencies and total cell voltages for different IEM-based CO_2RR reactors designed for CO or formate/formic acid production, some key insights are provided.

Figure 12a shows the FE of CO formation for different IEM systems. From this plot, it is clear that AEMs exhibit the highest FEs primarily due to the high pH conditions at the cathode, inhibiting the HER and enabling selective CO_2RRs. Notably, the FEs of CO_2 electrolyzers using BPMs under forward bias conditions are comparable to those using AEMs under optimized conditions that prevent salt precipitation at the bipolar junction [222]. CEMs and reverse bias BPMs typically demonstrate much lower FEs due to a more facile HER at low pH conditions. The low FEs for CO_2RRs are problematic if such

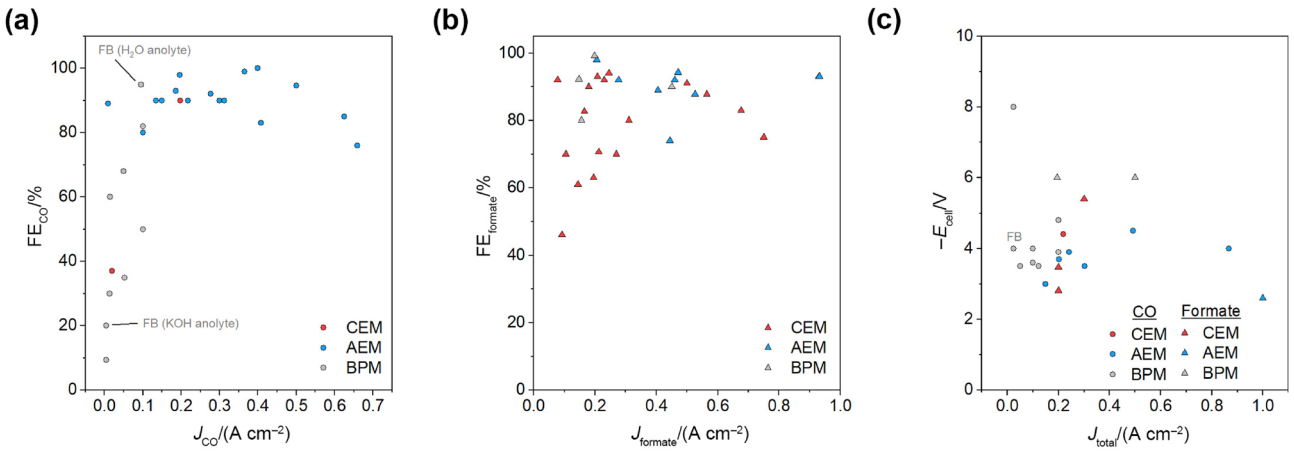

Fig. 12 Comparison of the performance levels of flow CO_2RR reactors with AEMs, CEMs and BPMs under reverse bias conditions (unless otherwise labeled FB) that produce **a** CO and **b** formate as their main products. In **c**, full-cell voltages of IEM-based flow CO_2RR reactors with various products are shown. (●) and (▲) represent devices that mainly produce CO and formate, respectively. Data are collected from the following references [26, 30, 65, 67, 70, 71, 167, 199, 200, 203, 232–266]

systems are adapted for C_{2+} products, which include more competing reaction pathways. Due to the high electrical cost of production, these products require much higher FEs than C_1 products for economic viability [43]. A similar comparison is made in Fig. 12b for the production of formate/formic acid. CEMs and BPMs (in reverse bias) allow high FEs in flow reactors that are predominantly used for CO_2RRs to formic acid conversion, due to their ability to inhibit the crossovers of anionic liquid products, including formate. For instance, an FE of 88% for $HCOO^-$ has been achieved in a Nafion-based flow CO_2 electrolyzer with Bi/Ag-modified graphite felt as the cathode and $KHCO_3$ catholyte/buffer solution (pH 7.2) at −1.6 V (vs. SCE) applied constant potential [267]. More recently, Kirner et al. have compared the formate production metrics of Bi-based and Sn-based catalysts in two flow cell designs employing CEM and BPM [268]. When Nafion (K^+-exchanged) membranes and 0.5 M $KHCO_3$ as both catholyte and anolyte are used, a total cell resistance of ~0.8 Ω (~5 Ω cm^2) is measured, and almost 95% $FE_{formate}$ has been obtained at 200 mA cm^{-2} with a full cell voltage of –3.6 V. The BPM-based membrane shows a high internal resistance [~1.2 Ω (~7.5 Ω cm^2)] despite using 0.5 M KOH as the anolyte, leading to a full cell voltage of –4.73 V; however, this membrane yields a slightly higher $FE_{formate}$ (97%) at 200 mA cm^{-2}. Overall, the authors have concluded that the higher EE obtained with the BPM (26%) relative to the CEM (22%) demonstrates the potential of these reactors to reach industrial standards upon further improvements in BPM developments that reduce voltage losses.

Figure 12c shows the cell voltages reported for the different IEM systems. Despite the high ionic conductivity, CEM systems exhibit higher cell voltages than AEMs, largely due to the high overvoltage required for the acidic OER, and the circulation a buffer catholyte, which is more typically used for CEMs than for AEMs which adds an additional ionic resistance to the reactor. AEM-based reactors typically yield cell voltages in the range of 2.5–4.0 V, but significantly lower voltages are observed for systems utilizing KOH anolytes due to the higher ionic conductivities of the liquid electrolytes (i.e., lower ohmic losses) and lower overpotentials required for alkaline OER. BPMs impose an additional voltage loss due to the presence of heterogenous junctions and energy consuming internal reactions (e.g., water dissociation in reverse bias mode); however, as mentioned in Sect. 3.3.1, this additional overpotential significantly decreases with state-of-the-art interfaces containing water dissociation catalysts. These advancements are expected to only be implemented in CO_2 electrolyzers when translated into commercially available products, since improving water dissociation at the interface is not typically the emphasis in CO_2RR studies that utilize BPMs.

4.2 Stability of IEMs

The main degradation pathways for IEMs are summarized in Table 3. As discussed in Sect. 3.1.4, the free radical-induced degradation characteristics of CEMs have not been reported in CO_2 electrolyzers; however, they are highly prevalent in PEMFCs. The lack of data to date makes quantitative comparison between the different IEMs problematic at this stage of CO_2 electrolyzer development. Nevertheless, it is known that many AEMs are susceptible to chemical degradation when employed in alkaline CO_2RR reactors, especially when concentrated

Table 3 Degradation mechanisms of IEMs and proposed synthetic approaches for mitigating degradation

IEM	Chemical degradation	Mitigation strategy
CEM	Degradation by hydroxyl ($HO^{\bullet}$) and peroxyl ($HO^{\bullet}_2$) radicals (as observed in PEMFCs)	Treatment with EDTA Imbibing with water-insoluble peroxyl inhibitors and radical scavengers
AEM	Hydroxide ion attack on the polymer (as found in alkaline electrolyzers)	Modifications of the chemical structure: Functional groups with steric hindrance of Hoffman elimination and other degradation mechanisms
BPM	Chemical stability of the polymer layers and the mechanical stability of the bipolar interface	Improvements in the chemical stability of the constituent IEMs and improvements in adhesion of the layers

alkaline solutions are present. The utilization of high concentrations of hydroxide salts is employed in laboratory-scale CO_2RR studies to reduce E_{cell} values, enhance the selectivity of multicarbon products, and increase the EE values [269–271]. Gewirth and their research team have reported that using 10 M KOH electrolytes in their AEM-based flow reactor yields 93% FE for C_2 products (87% ethylene and 6% ethanol) at 2.02 V cell potential, with 50% energetic efficiency [272]. This strategy, however, is not applicable to the vast majority of AEMs due to OH^- nucleophilic attack. Increasing the pH of anolytes can lead to other catastrophic phenomena impacting the operational stabilities of cells unless preventative measures, such as the regular removal of salt precipitates from the cathode or the refreshment of the pH of the electrolyte, are taken [273]. Therefore, high operational stabilities with AEMs are often obtained with low-concentration electrolytes. For example, when Sustainion® membranes are used in a CO_2 electrolyzer with 10 mM $KHCO_3$, an operational stability of 3 000 h is achieved at a low current density of 50 mA cm^{-2}. At 200 mA cm^{-2}, the operational stability is reported to reduce to 1 000 h using the same electrolyte [274].

The durability levels of BPMs are primarily dictated by the stability of the bipolar interface. The CELs of BPMs are usually stable in contact with neutral electrolyte solutions, such as those used in CEM-based CO_2RR reactors; however, many AELs degrade under caustic conditions. Moreover, differences in the CEL and AEL properties, such as swelling and mechanical strength, may lead to the delamination of the constituent layers [224]. The buildup of water at the bipolar interface under forward bias or the insufficient transport of water to the BPM interface under reverse bias may result in the delamination or mechanical deformation of the BPM, leading to considerable losses in electrochemical performance [131]. The adhesion of layers improves by increasing the interfacial surface areas between the layers by roughening the surfaces of the IEMs and developing a BPM from a single material [205].

5 Summary and Outlook

The further development of CO_2RR electrolyzers based on scalable flow reactors utilizing IEMs requires tailoring the membrane properties to meet the operational requirements to achieve the desired durability, selectivity, and efficiency characteristics. The design of the next-generation IEMs for CO_2 electrolysis should be focused on (1) reducing the crossover of coions to mitigate salt precipitation at the cathode; (2) reducing the carbonation in the membrane; (3) reducing the crossover of neutral products; (4) improving the chemical stability of membranes in alkaline media and at elevated temperatures; (5) optimizing water transport between the anode and cathode; and (6) maintaining high ionic conductivity to reduce ohmic losses.

Research on CEMs with reduced product crossover characteristics and on new cell designs allowing the adjustment of the cathode pH environment are two areas to consider when designing CEM-based CO_2 electrolyzers. An ideal CEM offers high conductivity and high permselectivity for protons at a low cost. Of the classes of IEMs discussed in this review, CEMs are the most mature. However, the acidic nature of the CEM typically necessitates the use of a buffer layer to mitigate the HER, which in turn results in an increase in the ohmic resistance of CO_2RR reactors and mitigates the benefits of the high CEM conductivity. The utilization of CEMs in flow electrolyzers might be improved by the careful engineering of a polymeric cation-augmenting layer between the electrode surface and the acidic electrolyte to increase the surface pH and hence the CO_2RR selectivity [96]. The diffusional crossover of neutral species during operation is a relatively unknown parameter at this stage that must be addressed and reduced without compromising ionic conductivity.

While implementation in zero-gap electrolyzers is feasible in AEM systems, electroosmotic drag facilitates neutral product crossover, which transverses in the same direction as the desired ionic transport. To address the crossovers of anionic species, such as bicarbonate, carbonate, and formate,

novel approaches, such as surface functionalization must be explored. Aside from considerations of chemical stability under caustic conditions, stability considerations must include coion diffusion leading to salt precipitation in the cathode catalyst layer.

To leverage the advantages afforded by BPMs, membrane interfaces promoting high rates of water dissociation, high ionic conductivity, and high selectivity (low coion leakage or ion crossover) are needed. The mechanical and chemical stabilities of the components are essential and dependent on the structural membrane layer properties. Offsetting the swelling ratios of individual layers promotes physical damage and delamination; thus, balancing the water content and conductivity levels of the individual membranes of the BPM are critical. Despite these challenges, recent advancements for reverse bias BPMs have achieved nearly equal membrane resistance levels to AEMs [56], and novel system designs for CO_2RR allow the use of forward bias BPMs [222]. Therefore, there is great promise in the BPM strategy; it is anticipated that if advancements in membrane technology and utilization are scaled, BPM-based CO_2RR reactors may achieve energetic efficiencies levels on par with AEM-based systems without deleterious carbonate formation and product crossover concerns.

Membrane-centric studies remain scarce in the CO_2RR literature; hence, there is a great need for research into ex situ testing protocols to evaluate both IEM stability and crossover characteristics under the conditions offered by a CO_2RR reactor. By developing an understanding of the structure–property–performance relationships of IEMs as applied to CO_2RR electrolyzers, IEMs specific to CO_2RR reactors can be developed. While the development of multiple reactor configurations has led to industrially applicable CO_2 electrolysis cells for various products, the further characterization of in situ membrane and ionomer degradation processes coinciding with long-term EE measurements is required to address key stability challenges needed to reach > 10 000 h. By providing an overview of the considerations for three main types of IEMs, this review aims to expedite these efforts.

Acknowledgements This work was funded by the National Research Council Canada's Materials for Clean Fuels Challenge Program (Collaborative Research Agreement: MCF-103-1 and Collaborative Research Agreement: M19-00570).

Funding Open Access funding provided by National Research Council Canada.

Declarations

Conflict of interest The authors declare no conflicts of interest.

References

1. Chu, S.: Carbon capture and sequestration. Science **325**, 1599 (2009). https://doi.org/10.1126/science.1181637
2. Beuttler, C., Charles, L., Wurzbacher, J.: The role of direct air capture in mitigation of anthropogenic greenhouse gas emissions. Front. Clim. **1**, 10 (2019). https://doi.org/10.3389/fclim.2019.00010
3. Al-Mamoori, A., Krishnamurthy, A., Rownaghi, A.A., et al.: Carbon capture and utilization update. Energy Technol. **5**, 834–849 (2017). https://doi.org/10.1002/ente.201600747
4. Baena-Moreno, F.M., Rodríguez-Galán, M., Vega, F., et al.: Carbon capture and utilization technologies: a literature review and recent advances. Energy Sources A Recovery Util Environ. Eff. **41**, 1403–1433 (2019)
5. Chemistry Industry Association of Canada: Chemistry: essential to Canada's transition to a low-carbon energy future. https://canadianchemistry.ca/wp-content/uploads/2021/09/CIAC_LowCarbonPaper_English_June2019_FINAL.pdf (2018)
6. Ravanchi, M.T., Sahebdelfar, S.: Carbon dioxide capture and utilization in petrochemical industry: potentials and challenges. Appl. Petrochem. Res. **4**, 63–77 (2014)
7. Griffin, P.W., Hammond, G.P., Norman, J.B.: Industrial energy use and carbon emissions reduction in the chemicals sector: a UK perspective. Appl. Energy **227**, 587–602 (2018). https://doi.org/10.1016/j.apenergy.2017.08.010
8. De Luna, P., Hahn, C., Higgins, D., et al.: What would it take for renewably powered electrosynthesis to displace petrochemical processes? Science **364**, eaav3506 (2019)
9. Teeter, T.E., Van Rysselberghe, P.: Reduction of carbon dioxide on mercury cathodes. J. Chem. Phys. **22**, 759–760 (1954). https://doi.org/10.1063/1.1740178
10. Russell, P.G., Kovac, N., Srinivasan, S., et al.: The electrochemical reduction of carbon dioxide, formic acid, and formaldehyde. J. Electrochem. Soc. **124**, 1329–1338 (1977). https://doi.org/10.1149/1.2133624
11. Udupa, K.S., Subramanian, G.S., Udupa, H.V.K.: The electrolytic reduction of carbon dioxide to formic acid. Electrochim. Acta **16**, 1593–1598 (1971). https://doi.org/10.1016/0013-4686(71)80028-2
12. Hori, Y., Kikuchi, K., Suzuki, S.: Production of CO and CH_4 in electrochemical reduction of CO_2 at metal electrodes in aqueous hydrogencarbonate solution. Chem. Lett. **14**, 1695–1698 (1985). https://doi.org/10.1246/cl.1985.1695
13. Hori, Y., Kikuchi, K., Murata, A., et al.: Production of methane and ethylene in electrochemical reduction of carbon dioxide at copper electrode in aqueous hydrogencarbonate solution. Chem. Lett. **15**, 897–898 (1986). https://doi.org/10.1246/cl.1986.897
14. Hori, Y., Murata, A., Takahashi, R., et al.: Enhanced formation of ethylene and alcohols at ambient temperature and pressure in electrochemical reduction of carbon dioxide at a copper

electrode. J. Chem. Soc. Chem. Commun. **1**, 17–19 (1988). https://doi.org/10.1039/c39880000017
15. Hori, Y., Wakebe, H., Tsukamoto, T., et al.: Electrocatalytic process of CO selectivity in electrochemical reduction of CO_2 at metal electrodes in aqueous media. Electrochim. Acta **39**, 1833–1839 (1994). https://doi.org/10.1016/0013-4686(94)85172-7
16. Hori, Y., Murata, A., Takahashi, R.: Formation of hydrocarbons in the electrochemical reduction of carbon dioxide at a copper electrode in aqueous solution. J. Chem. Soc. Faraday Trans. **85**, 2309 (1989). https://doi.org/10.1039/f19898502309
17. Hori, Y.: Electrochemical CO_2 reduction on metal electrodes. In: Vayenas, C.G., White, R.E., Gamboa-Aldeco, M.E. (eds.) Modern Aspects of Electrochemistry, pp. 89–189. Springer, New York (2008)
18. Nitopi, S., Bertheussen, E., Scott, S.B., et al.: Progress and perspectives of electrochemical CO_2 reduction on copper in aqueous electrolyte. Chem. Rev. **119**, 7610–7672 (2019). https://doi.org/10.1021/acs.chemrev.8b00705
19. Zhao, J., Xue, S., Barber, J., et al.: An overview of Cu-based heterogeneous electrocatalysts for CO_2 reduction. J. Mater. Chem. A **8**, 4700–4734 (2020). https://doi.org/10.1039/C9TA11778D
20. Usman, M., Humayun, M., Garba, M.D., et al.: Electrochemical reduction of CO_2: a review of cobalt based catalysts for carbon dioxide conversion to fuels. Nanomaterials (Basel) **11**, 2029 (2021)
21. Pei, Y.H., Zhong, H., Jin, F.M.: A brief review of electrocatalytic reduction of CO_2: materials, reaction conditions, and devices. Energy Sci. Eng. **9**, 1012–1032 (2021). https://doi.org/10.1002/ese3.935
22. Liu, A.M., Gao, M.F., Ren, X.F., et al.: Current progress in electrocatalytic carbon dioxide reduction to fuels on heterogeneous catalysts. J. Mater. Chem. A **8**, 3541–3562 (2020). https://doi.org/10.1039/C9TA11966C
23. Zhang, X.L., Guo, S.X., Gandionco, K.A., et al.: Electrocatalytic carbon dioxide reduction: from fundamental principles to catalyst design. Mater. Today. Adv. **7**, 100074 (2020). https://doi.org/10.1016/j.mtadv.2020.100074
24. Lees, E.W., Mowbray, B.A.W., Parlane, F.G.L., et al.: Gas diffusion electrodes and membranes for CO_2 reduction electrolysers. Nat. Rev. Mater. **7**, 55–64 (2022). https://doi.org/10.1038/s41578-021-00356-2
25. Ye, K., Zhang, G.R., Ma, X.Y., et al.: Resolving local reaction environment toward an optimized CO_2-to-CO conversion performance. Energy Environ. Sci. **15**, 749–759 (2022). https://doi.org/10.1039/D1EE02966E
26. Li, H., Oloman, C.: Development of a continuous reactor for the electro-reduction of carbon dioxide to formate. Part 2. Scale-up. J. Appl. Electrochem. **37**, 1107–1117 (2007). https://doi.org/10.1007/s10800-007-9371-8
27. Subramanian, K., Asokan, K., Jeevarathinam, D., et al.: Electrochemical membrane reactor for the reduction of carbon dioxide to formate. J. Appl. Electrochem. **37**, 255–260 (2007). https://doi.org/10.1007/s10800-006-9252-6
28. Weekes, D.M., Salvatore, D.A., Reyes, A., et al.: Electrolytic CO_2 reduction in a flow cell. Acc. Chem. Res. **51**, 910–918 (2018). https://doi.org/10.1021/acs.accounts.8b00010
29. Zhang, M., Wei, W.B., Zhou, S.H., et al.: Engineering a conductive network of atomically thin bismuthene with rich defects enables CO_2 reduction to formate with industry-compatible current densities and stability. Energy Environ. Sci. **14**, 4998–5008 (2021). https://doi.org/10.1039/D1EE01495A
30. Delacourt, C., Ridgway, P.L., Kerr, J.B., et al.: Design of an electrochemical cell making syngas ($CO + H_2$) from CO_2 and H_2O reduction at room temperature. J. Electrochem. Soc. **155**, B42 (2008). https://doi.org/10.1149/1.2801871
31. Narayanan, S.R., Haines, B., Soler, J., et al.: Electrochemical conversion of carbon dioxide to formate in alkaline polymer electrolyte membrane cells. J. Electrochem. Soc. **158**, A167 (2011). https://doi.org/10.1149/1.3526312
32. Whipple, D.T., Finke, E.C., Kenis, P.J.A.: Microfluidic reactor for the electrochemical reduction of carbon dioxide: the effect of pH. Electrochem. Solid State Lett. **13**, B109 (2010). https://doi.org/10.1149/1.3456590
33. Shironita, S., Karasuda, K., Sato, K., et al.: Methanol generation by CO_2 reduction at a Pt–Ru/C electrocatalyst using a membrane electrode assembly. J. Power Sources **240**, 404–410 (2013). https://doi.org/10.1016/j.jpowsour.2013.04.034
34. Lee, S., Ocon, J.D., Son, Y.I., et al.: Alkaline CO_2 electrolysis toward selective and continuous $HCOO^-$ production over SnO_2 nanocatalysts. J. Phys. Chem. C **119**, 4884–4890 (2015). https://doi.org/10.1021/jp512436w
35. Surya Prakash, G.K., Viva, F.A., Olah, G.A.: Electrochemical reduction of CO_2 over Sn-Nafion® coated electrode for a fuel-cell-like device. J. Power Sources **223**, 68–73 (2013). https://doi.org/10.1016/j.jpowsour.2012.09.036
36. Li, Y.C., Zhou, D.K., Yan, Z.F., et al.: Electrolysis of CO_2 to syngas in bipolar membrane-based electrochemical cells. ACS Energy Lett. **1**, 1149–1153 (2016). https://doi.org/10.1021/acsenergylett.6b00475
37. Masel, R.I., Liu, Z.C., Sajjad, S.: Anion exchange membrane electrolyzers showing 1 A cm^{-2} at less than 2 V. ECS Trans. **75**, 1143–1146 (2016). https://doi.org/10.1149/07514.1143ecst
38. Shao, B., Zhang, Y., Sun, Z.Y., et al.: CO_2 capture and in-situ conversion: recent progresses and perspectives. Green Chem. Eng. **3**, 189–198 (2022). https://doi.org/10.1016/j.gce.2021.11.009
39. Matin, A.J., Larrazábal, G.O., Pérez-Ramírez, J.: Towards sustainable fuels and chemicals through the electrochemical reduction of CO_2: lessons from water electrolysis. Green Chem. **17**, 5114–5130 (2015). https://doi.org/10.1039/C5GC01893E
40. Hydrogen and Fuel Cell Technologies Office: DOE technical targets for hydrogen production from electrolysis. https://www.energy.gov/eere/fuelcells/hydrogen-production-electrolysis
41. Verma, S., Kim, B., Jhong, H.R.M., et al.: A gross-margin model for defining technoeconomic benchmarks in the electroreduction of CO_2. ChemSusChem **9**, 1972–1979 (2016). https://doi.org/10.1002/cssc.201600394
42. Bushuyev, O.S., De Luna, P., Dinh, C.T., et al.: What should we make with CO_2 and how can we make it? Joule **2**, 825–832 (2018). https://doi.org/10.1016/j.joule.2017.09.003
43. Jouny, M., Luc, W., Jiao, F.: General techno-economic analysis of CO_2 electrolysis systems. Ind. Eng. Chem. Res. **57**, 2165–2177 (2018). https://doi.org/10.1021/acs.iecr.7b03514
44. Verma, S., Lu, S., Kenis, P.J.A.: Co-electrolysis of CO_2 and glycerol as a pathway to carbon chemicals with improved technoeconomics due to low electricity consumption. Nat. Energy **4**, 466–474 (2019). https://doi.org/10.1038/s41560-019-0374-6
45. Yadegari, H., Ozden, A., Alkayyali, T., et al.: Glycerol oxidation pairs with carbon monoxide reduction for low-voltage generation of C_2 and C_3 product streams. ACS Energy Lett. **6**, 3538–3544 (2021). https://doi.org/10.1021/acsenergylett.1c01639
46. Endrődi, B., Kecsenovity, E., Samu, A., et al.: High carbonate ion conductance of a robust PiperION membrane allows industrial current density and conversion in a zero-gap carbon dioxide electrolyzer cell. Energy Environ. Sci. **13**, 4098–4105 (2020). https://doi.org/10.1039/D0EE02589E
47. Liang, S.Y., Altaf, N., Huang, L., et al.: Electrolytic cell design for electrochemical CO_2 reduction. J. CO2 Util. **35**, 90–105 (2020). https://doi.org/10.1016/j.jcou.2019.09.007

48. Chaplin, R.P.S., Wragg, A.A.: Effects of process conditions and electrode material on reaction pathways for carbon dioxide electroreduction with particular reference to formate formation. J. Appl. Electrochem. **33**, 1107–1123 (2003). https://doi.org/10.1023/B:JACH.0000004018.57792.b8
49. Varela, A.S.: The importance of pH in controlling the selectivity of the electrochemical CO_2 reduction. Curr. Opin. Green Sustain. Chem. **26**, 100371 (2020). https://doi.org/10.1016/j.cogsc.2020.100371
50. Zhang, Z.S., Melo, L., Jansonius, R.P., et al.: pH matters when reducing CO_2 in an electrochemical flow cell. ACS Energy Lett. **5**, 3101–3107 (2020). https://doi.org/10.1021/acsenergylett.0c01606
51. Vennekoetter, J.B., Sengpiel, R., Wessling, M.: Beyond the catalyst: how electrode and reactor design determine the product spectrum during electrochemical CO_2 reduction. Chem. Eng. J. **364**, 89–101 (2019). https://doi.org/10.1016/j.cej.2019.01.045
52. Varcoe, J.R., Atanassov, P., Dekel, D.R., et al.: Anion-exchange membranes in electrochemical energy systems. Energy Environ. Sci. **7**, 3135–3191 (2014). https://doi.org/10.1039/C4EE01303D
53. Du, N.Y., Roy, C., Peach, R., et al.: Anion-exchange membrane water electrolyzers. Chem. Rev. **122**, 11830–11895 (2022). https://doi.org/10.1021/acs.chemrev.1c00854
54. Vermaas, D.A., Smith, W.A.: Synergistic electrochemical CO_2 reduction and water oxidation with a bipolar membrane. ACS Energy Lett. **1**, 1143–1148 (2016). https://doi.org/10.1021/acsenergylett.6b00557
55. Pärnamäe, R., Mareev, S., Nikonenko, V., et al.: Bipolar membranes: a review on principles, latest developments, and applications. J. Membr. Sci. **617**, 118538 (2021). https://doi.org/10.1016/j.memsci.2020.118538
56. Oener, S.Z., Foster, M.J., Boettcher, S.W.: Accelerating water dissociation in bipolar membranes and for electrocatalysis. Science **369**, 1099–1103 (2020). https://doi.org/10.1126/science.aaz1487
57. Hohenadel, A., Powers, D., Wycisk, R., et al.: Electrochemical characterization of hydrocarbon bipolar membranes with varying junction morphology. ACS Appl. Energy Mater. **2**, 6817–6824 (2019). https://doi.org/10.1021/acsaem.9b01257
58. Li, T.F., Lees, E.W., Zhang, Z.S., et al.: Conversion of bicarbonate to formate in an electrochemical flow reactor. ACS Energy Lett. **5**, 2624–2630 (2020). https://doi.org/10.1021/acsenergylett.0c01291
59. Küngas, R.: Review—electrochemical CO_2 reduction for CO production: comparison of low- and high-temperature electrolysis technologies. J. Electrochem. Soc. **167**, 044508 (2020). https://doi.org/10.1149/1945-7111/ab7099
60. Salvatore, D.A., Gabardo, C.M., Reyes, A., et al.: Designing anion exchange membranes for CO_2 electrolysers. Nat. Energy **6**, 339–348 (2021). https://doi.org/10.1038/s41560-020-00761-x
61. Chen, N.J., Wang, H.H., Kim, S.P., et al.: Poly(fluorenyl aryl piperidinium) membranes and ionomers for anion exchange membrane fuel cells. Nat. Commun. **12**, 2367 (2021). https://doi.org/10.1038/s41467-021-22612-3
62. Ran, J., Wu, L., He, Y.B., et al.: Ion exchange membranes: new developments and applications. J. Membr. Sci. **522**, 267–291 (2017). https://doi.org/10.1016/j.memsci.2016.09.033
63. Dang, H.S., Jannasch, P.: A comparative study of anion-exchange membranes tethered with different hetero-cycloaliphatic quaternary ammonium hydroxides. J. Mater. Chem. A **5**, 21965–21978 (2017). https://doi.org/10.1039/C7TA06029G
64. Kusoglu, A., Weber, A.Z.: New insights into perfluorinated sulfonic-acid ionomers. Chem. Rev. **117**, 987–1104 (2017). https://doi.org/10.1021/acs.chemrev.6b00159
65. Duarte, M., De Mot, B., Hereijgers, J., et al.: Electrochemical reduction of CO_2: effect of convective CO_2 supply in gas diffusion electrodes. ChemElectroChem **6**, 5596–5602 (2019). https://doi.org/10.1002/celc.201901454
66. Zhang, X., Li, J.C., Li, Y.Y., et al.: Selective and high current CO_2 electro-reduction to multicarbon products in near-neutral KCl electrolytes. J. Am. Chem. Soc. **143**, 3245–3255 (2021). https://doi.org/10.1021/jacs.0c13427
67. Sen, S., Brown, S.M., Leonard, M., et al.: Electroreduction of carbon dioxide to formate at high current densities using tin and tin oxide gas diffusion electrodes.J. Appl. Electrochem. **49**, 917–928 (2019). https://doi.org/10.1007/s10800-019-01332-z
68. Gabardo, C.M., O'Brien, C.P., Edwards, J.P., et al.: Continuous carbon dioxide electroreduction to concentrated multi-carbon products using a membrane electrode assembly. Joule **3**, 2777–2791 (2019). https://doi.org/10.1016/j.joule.2019.07.021
69. Kaczur, J.J., Yang, H.Z., Liu, Z.C., et al.: Carbon dioxide and water electrolysis using new alkaline stable anion membranes. Front. Chem. **6**, 263 (2018). https://doi.org/10.3389/fchem.2018.00263
70. Chen, K.J., Cao, M.Q., Lin, Y.Y., et al.: Ligand engineering in nickel phthalocyanine to boost the electrocatalytic reduction of CO_2. Adv. Funct. Mater. **32**, 2111322 (2022). https://doi.org/10.1002/adfm.202111322
71. Lees, E.W., Goldman, M., Fink, A.G., et al.: Electrodes designed for converting bicarbonate into CO. ACS Energy Lett. **5**, 2165–2173 (2020). https://doi.org/10.1021/acsenergylett.0c00898
72. Ramdin, M., Morrison, A.R.T., de Groen, M., et al.: High pressure electrochemical reduction of CO_2 to formic acid/formate: a comparison between bipolar membranes and cation exchange membranes. Ind. Eng. Chem. Res. **58**, 1834–1847 (2019). https://doi.org/10.1021/acs.iecr.8b04944
73. He, G.W., Li, Z., Zhao, J., et al.: Nanostructured ion-exchange membranes for fuel cells: recent advances and perspectives. Adv. Mater. **27**, 5280–5295 (2015). https://doi.org/10.1002/adma.201501406
74. Hou, Y., Liang, Y.L., Shi, P.C., et al.: Atomically dispersed Ni species on N-doped carbon nanotubes for electroreduction of CO_2 with nearly 100% CO selectivity. Appl. Catal. B Environ. **271**, 118929 (2020). https://doi.org/10.1016/j.apcatb.2020.118929
75. Zhou, Y., Zhou, R., Zhu, X.R., et al.: Mesoporous PdAg nanospheres for stable electrochemical CO_2 reduction to formate. Adv. Mater. **32**, e2000992 (2020). https://doi.org/10.1002/adma.202000992
76. Tang, J.K., Zhu, C.Y., Jiang, T.W., et al.: Anion exchange-induced single-molecule dispersion of cobalt porphyrins in a cationic porous organic polymer for enhanced electrochemical CO_2 reduction via secondary-coordination sphere interactions. J. Mater. Chem. A **8**, 18677–18686 (2020). https://doi.org/10.1039/D0TA07068H
77. Lv, X.M., Shang, L.M., Zhou, S., et al.: Electron-deficient Cu sites on Cu_3Ag_1 catalyst promoting CO_2 electroreduction to alcohols. Adv. Energy Mater. **10**, 2001987 (2020). https://doi.org/10.1002/aenm.202001987
78. Ma, W.C., Xie, S.J., Liu, T.T., et al.: Electrocatalytic reduction of CO_2 to ethylene and ethanol through hydrogen-assisted C–C coupling over fluorine-modified copper. Nat. Catal. **3**, 478–487 (2020). https://doi.org/10.1038/s41929-020-0450-0
79. Sato, M., Ogihara, H., Yamanaka, I.: Electrocatalytic reduction of CO_2 to CO and CH_4 by Co–N–C catalyst and Ni co-catalyst with PEM reactor. ISIJ Int. **59**, 623–627 (2019). https://doi.org/10.2355/isijinternational.isijint-2018-551
80. Zhang, Z.S., Lees, E.W., Ren, S.X., et al.: Conversion of reactive carbon solutions into CO at low voltage and high carbon efficiency. ACS Cent. Sci. **8**, 749–755 (2022). https://doi.org/10.1021/acscentsci.2c00329

81. Ogungbemi, E., Ijaodola, O., Khatib, F.N., et al.: Fuel cell membranes: pros and cons. Energy **172**, 155–172 (2019). https://doi.org/10.1016/j.energy.2019.01.034
82. junge Puring, K., Evers, O., Prokein, M., et al.: Assessing the influence of supercritical carbon dioxide on the electrochemical reduction to formic acid using carbon-supported copper catalysts. ACS Catal. **10**, 12783–12789 (2020). https://doi.org/10.1021/acscatal.0c02983
83. Rasul, S., Pugnant, A., Xiang, H., et al.: Low cost and efficient alloy electrocatalysts for CO_2 reduction to formate. J. CO2 Util. **32**, 1–10 (2019). https://doi.org/10.1016/j.jcou.2019.03.016
84. Bose, S., Kuila, T., Nguyen, T.X.H., et al.: Polymer membranes for high temperature proton exchange membrane fuel cell: recent advances and challenges. Prog. Polym. Sci. **36**, 813–843 (2011). https://doi.org/10.1016/j.progpolymsci.2011.01.003
85. Gutiérrez-Guerra, N., Valverde, J.L., Romero, A., et al.: Electrocatalytic conversion of CO_2 to added-value chemicals in a high-temperature proton-exchange membrane reactor. Electrochem. Commun. **81**, 128–131 (2017). https://doi.org/10.1016/j.elecom.2017.06.018
86. Luo, T., Abdu, S., Wessling, M.: Selectivity of ion exchange membranes: a review. J. Membr. Sci. **555**, 429–454 (2018). https://doi.org/10.1016/j.memsci.2018.03.051
87. Kamcev, J., Paul, D.R., Manning, G.S., et al.: Ion diffusion coefficients in ion exchange membranes: significance of counterion condensation. Macromolecules **51**, 5519–5529 (2018). https://doi.org/10.1021/acs.macromol.8b00645
88. Thampan, T., Malhotra, S., Tang, H., et al.: Modeling of conductive transport in proton-exchange membranes for fuel cells. J. Electrochem. Soc. **147**, 3242 (2000). https://doi.org/10.1149/1.1393890
89. Weng, L.C., Bell, A.T., Weber, A.Z.: Towards membrane-electrode assembly systems for CO_2 reduction: a modeling study. Energy Environ. Sci. **12**, 1950–1968 (2019). https://doi.org/10.1039/C9EE00909D
90. Peckham, T.J., Holdcroft, S.: Structure-morphology-property relationships of non-perfluorinated proton-conducting membranes. Adv. Mater. **22**, 4667–4690 (2010). https://doi.org/10.1002/adma.201001164
91. DeLuca, N.W., Elabd, Y.A.: Polymer electrolyte membranes for the direct methanol fuel cell: a review. J. Polym. Sci. B Polym. Phys. **44**, 2201–2225 (2006). https://doi.org/10.1002/polb.20861
92. Choi, P., Jalani, N.H., Datta, R.: Thermodynamics and proton transport in Nafion. J. Electrochem. Soc. **152**, E123 (2005). https://doi.org/10.1149/1.1859814
93. Hickner, M.A.: Ion-containing polymers: new energy & clean water. Mater. Today **13**, 34–41 (2010). https://doi.org/10.1016/S1369-7021(10)70082-1
94. Ersöz, M.: Diffusion and selective transport of alkali cations on cation-exchange membrane. Sep. Sci. Technol. **30**, 3523–3533 (1995). https://doi.org/10.1080/01496399508015133
95. Liao, W.C., Tsai, D.H., Hong, W.Z., et al.: Enabling direct CO_2 electrolysis by alkali metal cation substituted membranes in a gas diffusion electrode reactor. Chem. Eng. J. **434**, 134765 (2022). https://doi.org/10.1016/j.cej.2022.134765
96. Huang, J.E., Li, F.W., Ozden, A., et al.: CO_2 electrolysis to multicarbon products in strong acid. Science **372**, 1074–1078 (2021). https://doi.org/10.1126/science.abg6582
97. Resasco, J., Chen, L.D., Clark, E., et al.: Promoter effects of alkali metal cations on the electrochemical reduction of carbon dioxide. J. Am. Chem. Soc. **139**, 11277–11287 (2017). https://doi.org/10.1021/jacs.7b06765
98. Ringe, S., Clark, E.L., Resasco, J., et al.: Understanding cation effects in electrochemical CO_2 reduction. Energy Environ. Sci. **12**, 3001–3014 (2019). https://doi.org/10.1039/C9EE01341E
99. Alerte, T., Edwards, J.P., Gabardo, C.M., et al.: Downstream of the CO_2 electrolyzer: assessing the energy intensity of product separation. ACS Energy Lett. **6**, 4405–4412 (2021). https://doi.org/10.1021/acsenergylett.1c02263
100. Wang, N., MiaoLee, rkG., et al.: Suppressing the liquid product crossover in electrochemical CO_2 reduction. SmartMat **2**, 12–16 (2021). https://doi.org/10.1002/smm2.1018
101. Zhang, J., Luo, W., Züttel, A.: Crossover of liquid products from electrochemical CO_2 reduction through gas diffusion electrode and anion exchange membrane. J. Catal. **385**, 140–145 (2020). https://doi.org/10.1016/j.jcat.2020.03.013
102. Tschinder, T., Schaffer, T., Fraser, S.D., et al.: Electro-osmotic drag of methanol in proton exchange membranes. J. Appl. Electrochem. **37**, 711–716 (2007). https://doi.org/10.1007/s10800-007-9304-6
103. Neburchilov, V., Martin, J., Wang, H.J., et al.: A review of polymer electrolyte membranes for direct methanol fuel cells. J. Power Sources **169**, 221–238 (2007). https://doi.org/10.1016/j.jpowsour.2007.03.044
104. Heinzel, A., Barragán, V.M.: A review of the state-of-the-art of the methanol crossover in direct methanol fuel cells. J. Power Sources **84**, 70–74 (1999). https://doi.org/10.1016/S0378-7753(99)00302-X
105. Awang, N., Ismail, A.F., Jaafar, J., et al.: Functionalization of polymeric materials as a high performance membrane for direct methanol fuel cell: a review. React. Funct. Polym. **86**, 248–258 (2015). https://doi.org/10.1016/j.reactfunctpolym.2014.09.019
106. Ahmad, H., Kamarudin, S.K., Hasran, U.A., et al.: Overview of hybrid membranes for direct-methanol fuel-cell applications. Int. J. Hydrog. Energy **35**, 2160–2175 (2010). https://doi.org/10.1016/j.ijhydene.2009.12.054
107. Antonucci, P.L., Aricò, A.S., Cretì, P., et al.: Investigation of a direct methanol fuel cell based on a composite Nafion®-silica electrolyte for high temperature operation. Solid State Ion. **125**, 431–437 (1999). https://doi.org/10.1016/S0167-2738(99)00206-4
108. Vaivars, G., Maxakato, N.W., Mokrani, T., et al.: Zirconium phosphate based inorganic direct methanol fuel cell. Mater. Sci. **10**, 162–165 (2004)
109. Rao, A.S., Rashmi, K.R., Manjunatha, D.V., et al.: Methanol crossover reduction and power enhancement of methanol fuel cells with polyvinyl alcohol coated Nafion membranes. Mater. Today Proc. **35**, 344–351 (2021). https://doi.org/10.1016/j.matpr.2020.02.093
110. Chabi, S., Papadantonakis, K.M., Lewis, N.S., et al.: Membranes for artificial photosynthesis. Energy Environ. Sci. **10**, 1320–1338 (2017). https://doi.org/10.1039/C7EE00294G
111. Burton, N.A., Padilla, R.V., Rose, A., et al.: Increasing the efficiency of hydrogen production from solar powered water electrolysis. Renew. Sustain. Energy Rev. **135**, 110255 (2021). https://doi.org/10.1016/j.rser.2020.110255
112. Masel, R.I., Liu, Z.C., Yang, H.Z., et al.: An industrial perspective on catalysts for low-temperature CO_2 electrolysis. Nat. Nanotechnol. **16**, 118–128 (2021). https://doi.org/10.1038/s41565-020-00823-x
113. ZatoÅ, M., RoziÃ¨re, J., Jones, D.J.: Current understanding of chemical degradation mechanisms of perfluorosulfonic acid membranes and their mitigation strategies: a review. Sustain. Energy Fuels **1**, 409–438 (2017). https://doi.org/10.1039/C7SE00038C
114. Papakonstantinou, G., Algara-Siller, G., Teschner, D., et al.: Degradation study of a proton exchange membrane water electrolyzer

under dynamic operation conditions. Appl. Energy **280**, 115911 (2020). https://doi.org/10.1016/j.apenergy.2020.115911
115. Inaba, M., Kinumoto, T., Kiriake, M., et al.: Gas crossover and membrane degradation in polymer electrolyte fuel cells. Electrochim. Acta **51**, 5746–5753 (2006). https://doi.org/10.1016/j.electacta.2006.03.008
116. Grigoriev, S.A., Dzhus, K.A., Bessarabov, D.G., et al.: Failure of PEM water electrolysis cells: case study involving anode dissolution and membrane thinning. Int. J. Hydrog. Energy **39**, 20440–20446 (2014). https://doi.org/10.1016/j.ijhydene.2014.05.043
117. Maurya, S., Shin, S.H., Kim, Y., et al.: A review on recent developments of anion exchange membranes for fuel cells and redox flow batteries. RSC Adv. **5**, 37206–37230 (2015). https://doi.org/10.1039/C5RA04741B
118. Laconti, A., Liu, H., Mittelsteadt, C., et al.: Polymer electrolyte membrane degradation mechanisms in fuel cells: findings over the past 30 years and comparison with electrolyzers. ECS Trans. **1**, 199–219 (2006). https://doi.org/10.1149/1.2214554
119. Yamazaki, K.: High proton conductive and low gas permeable sulfonated graft copolyimide membrane. Macromolecules **43**, 7185–7191 (2010)
120. Adamski, M., Skalski, T.J.G., Britton, B., et al.: Highly stable, low gas crossover, proton-conducting phenylated polyphenylenes. Angew. Chem. Int. Ed. **56**, 9058–9061 (2017). https://doi.org/10.1002/anie.201703916
121. Adamski, M., Peressin, N., Holdcroft, S.: On the evolution of sulfonated polyphenylenes as proton exchange membranes for fuel cells. Mater. Adv. **2**, 4966–5005 (2021). https://doi.org/10.1039/d1ma00511a
122. Klose, C., Saatkamp, T., Münchinger, A., et al.: All-hydrocarbon MEA for PEM water electrolysis combining low hydrogen crossover and high efficiency. Adv. Energy Mater. **10**, 1903995 (2020). https://doi.org/10.1002/aenm.201903995
123. Besha, A.T., Tsehaye, M.T., Aili, D., et al.: Design of monovalent ion selective membranes for reducing the impacts of multivalent ions in reverse electrodialysis. Membranes **10**, 7 (2019). https://doi.org/10.3390/membranes10010007
124. Safronova, E.Y., Golubenko, D.V., Shevlyakova, N.V., et al.: New cation-exchange membranes based on cross-linked sulfonated polystyrene and polyethylene for power generation systems. J. Membr. Sci. **515**, 196–203 (2016). https://doi.org/10.1016/j.memsci.2016.05.006
125. Kienitz, B., Kolde, J., Priester, S., et al.: Ultra-thin reinforced ionomer membranes to meet next generation fuel cell targets. ECS Trans. **41**, 1521–1530 (2011). https://doi.org/10.1149/1.3635683
126. Li, D.G., Motz, A.R., Bae, C., et al.: Durability of anion exchange membrane water electrolyzers. Energy Environ. Sci. **14**, 3393–3419 (2021). https://doi.org/10.1039/d0ee04086j
127. Wang, Y.X., Niu, C.L., Zhu, Y.C., et al.: Tunable syngas formation from electrochemical CO_2 reduction on copper nanowire arrays. ACS Appl. Energy Mater. **3**, 9841–9847 (2020). https://doi.org/10.1021/acsaem.0c01504
128. He, M., Li, C.S., Zhang, H.C., et al.: Oxygen induced promotion of electrochemical reduction of CO_2 via co-electrolysis. Nat. Commun. **11**, 3844 (2020). https://doi.org/10.1038/s41467-020-17690-8
129. Liu, X.Y., Schlexer, P., Xiao, J.P., et al.: pH effects on the electrochemical reduction of CO_2 towards C_2 products on stepped copper. Nat. Commun. **10**, 32 (2019). https://doi.org/10.1038/s41467-018-07970-9
130. Chen, Z.P., Zhang, X.X., Liu, W., et al.: Amination strategy to boost the CO_2 electroreduction current density of M-N/C single-atom catalysts to the industrial application level. Energy Environ. Sci. **14**, 2349–2356 (2021). https://doi.org/10.1039/D0EE04052E
131. O'Brien, C.P., MiaoLiu, rkS.J., et al.: Single pass CO_2 conversion exceeding 85% in the electrosynthesis of multicarbon products via local CO_2 regeneration. ACS Energy Lett. **6**, 2952–2959 (2021). https://doi.org/10.1021/acsenergylett.1c01122
132. Niu, Z.Z., Chi, L.P., Liu, R., et al.: Rigorous assessment of CO_2 electroreduction products in a flow cell. Energy Environ. Sci. **14**, 4169–4176 (2021). https://doi.org/10.1039/D1EE01664D
133. Ma, M., Clark, E.L., Therkildsen, K.T., et al.: Insights into the carbon balance for CO_2 electroreduction on Cu using gas diffusion electrode reactor designs. Energy Environ. Sci. **13**, 977–985 (2020). https://doi.org/10.1039/D0EE00047G
134. Ma, M., Kim, S., Chorkendorff, I., et al.: Role of ion-selective membranes in the carbon balance for CO_2 electroreduction via gas diffusion electrode reactor designs. Chem. Sci. **11**, 8854–8861 (2020). https://doi.org/10.1039/d0sc03047c
135. Mardle, P., Cassegrain, S., Habibzadeh, F., et al.: Carbonate ion crossover in zero-gap, KOH anolyte CO_2 electrolysis. J. Phys. Chem. C **125**, 25446–25454 (2021). https://doi.org/10.1021/acs.jpcc.1c08430
136. Lee, W.H., Ko, Y.J., Choi, Y., et al.: Highly selective and scalable CO_2 to CO: electrolysis using coral-nanostructured Ag catalysts in zero-gap configuration. Nano Energy **76**, 105030 (2020). https://doi.org/10.1016/j.nanoen.2020.105030
137. Wei, P.F., Li, H.F., Lin, L., et al.: CO_2 electrolysis at industrial current densities using anion exchange membrane based electrolyzers. Sci. China Chem. **63**, 1711–1715 (2020)
138. Wheeler, D.G., Mowbray, B.A.W., Reyes, A., et al.: Quantification of water transport in a CO_2 electrolyzer. Energy Environ. Sci. **13**, 5126–5134 (2020). https://doi.org/10.1039/D0EE02219E
139. Leonard, M.E., Clarke, L.E., Forner-Cuenca, A., et al.: Investigating electrode flooding in a flowing electrolyte, gas-fed carbon dioxide electrolyzer. Chemsuschem **13**, 400–411 (2020). https://doi.org/10.1002/cssc.201902547
140. Aeshala, L.M., Verma, A.: Amines as reaction environment regulator for CO_2 electrochemical reduction to CH_4. Macromol. Symp. **357**, 79–85 (2015). https://doi.org/10.1002/masy.201400193
141. Aeshala, L.M., Uppaluri, R., Verma, A.: Electrochemical conversion of CO_2 to fuels: tuning of the reaction zone using suitable functional groups in a solid polymer electrolyte. Phys. Chem. Chem. Phys. **16**, 17588–17594 (2014). https://doi.org/10.1039/C4CP02389G
142. Mao, M.J., Zhang, M.D., Meng, D.L., et al.: Imidazolium-functionalized cationic covalent triazine frameworks stabilized copper nanoparticles for enhanced CO_2 electroreduction. ChemCatChem **12**, 3530–3536 (2020). https://doi.org/10.1002/cctc.202000387
143. Li, X.Q., Duan, G.Y., Chen, J.W., et al.: Regulating electrochemical CO_2RR selectivity at industrial current densities by structuring copper@poly(ionic liquid) interface. Appl. Catal. B Environ. **297**, 120471 (2021). https://doi.org/10.1016/j.apcatb.2021.120471
144. Ratschmeier, B., Braunschweig, B.: Cations of ionic liquid electrolytes can act as a promoter for CO_2 electrocatalysis through reactive intermediates and electrostatic stabilization. J. Phys. Chem. C **125**, 16498–16507 (2021). https://doi.org/10.1021/acs.jpcc.1c02898
145. Rosen, B.A., Salehi-Khojin, A., Thorson, M.R., et al.: Ionic liquid-mediated selective conversion of CO_2 to CO at low overpotentials. Science **334**, 643–644 (2011). https://doi.org/10.1126/science.1209786
146. Kemna, A., García Rey, N., Braunschweig, B.: Mechanistic insights on CO_2 reduction reactions at platinum/[BMIM][BF_4] interfaces from in operando spectroscopy. ACS Catal. **9**, 6284–6292 (2019). https://doi.org/10.1021/acscatal.9b01033

147. Tanner, E.E.L., Batchelor-McAuley, C., Compton, R.G.: Carbon dioxide reduction in room-temperature ionic liquids: the effect of the choice of electrode material, cation, and anion. J. Phys. Chem. C **120**, 26442–26447 (2016). https://doi.org/10.1021/acs.jpcc.6b10564
148. Sajjad, S.D., Gao, Y., Liu, Z.C., et al.: Tunable-high performance sustainion™ anion exchange membranes for electrochemical applications. ECS Trans. **77**, 1653–1656 (2017). https://doi.org/10.1149/07711.1653ecst
149. Yin, Z.L., Peng, H.Q., Wei, X., et al.: An alkaline polymer electrolyte CO_2 electrolyzer operated with pure water. Energy Environ. Sci. **12**, 2455–2462 (2019). https://doi.org/10.1039/C9EE01204D
150. Giffin, G.A., Lavina, S., Pace, G., et al.: Interplay between the structure and relaxations in Selemion AMV hydroxide conducting membranes for AEMFC applications. J. Phys. Chem. C **116**, 23965–23973 (2012). https://doi.org/10.1021/jp3094879
151. Carter, B.M., Dobyns, B.M., Beckingham, B.S., et al.: Multicomponent transport of alcohols in an anion exchange membrane measured by in-situ ATR FTIR spectroscopy. Polymer **123**, 144–152 (2017). https://doi.org/10.1016/j.polymer.2017.06.070
152. Krödel, M., Carter, B.M., Rall, D., et al.: Rational design of ion exchange membrane material properties limits the crossover of CO_2 reduction products in artificial photosynthesis devices. ACS Appl. Mater. Interfaces **12**, 12030–12042 (2020). https://doi.org/10.1021/acsami.9b21415
153. Carmo, M., Doubek, G., Sekol, R.C., et al.: Development and electrochemical studies of membrane electrode assemblies for polymer electrolyte alkaline fuel cells using FAA membrane and ionomer. J. Power Sources **230**, 169–175 (2013). https://doi.org/10.1016/j.jpowsour.2012.12.015
154. Ziv, N., Mondal, A.N., Weissbach, T., et al.: Effect of CO_2 on the properties of anion exchange membranes for fuel cell applications. J. Membr. Sci. **586**, 140–150 (2019). https://doi.org/10.1016/j.memsci.2019.05.053
155. Torbensen, K., Joulié, D., Ren, S.X., et al.: Molecular catalysts boost the rate of electrolytic CO_2 reduction. ACS Energy Lett. **5**, 1512–1518 (2020). https://doi.org/10.1021/acsenergylett.0c00536
156. Larrazábal, G.O., Strøm-Hansen, P., Heli, J.P., et al.: Analysis of mass flows and membrane cross-over in CO_2 reduction at high current densities in an MEA-type electrolyzer. ACS Appl. Mater. Interfaces **11**, 41281–41288 (2019). https://doi.org/10.1021/acsami.9b13081
157. Lees, E.W., Mowbray, B.A.W., Salvatore, D.A., et al.: Linking gas diffusion electrode composition to CO_2 reduction in a flow cell. J. Mater. Chem. A **8**, 19493–19501 (2020). https://doi.org/10.1039/D0TA03570J
158. Liu, Z.C., Yang, H.Z., Kutz, R., et al.: CO_2 electrolysis to CO and O_2 at high selectivity, stability and efficiency using Sustainion membranes. J. Electrochem. Soc. **165**, J3371–J3377 (2018). https://doi.org/10.1149/2.0501815jes
159. Durst, J., Siebel, A., Simon, C., et al.: New insights into the electrochemical hydrogen oxidation and evolution reaction mechanism. Energy Environ. Sci. **7**, 2255–2260 (2014). https://doi.org/10.1039/C4EE00440J
160. Feaster, J.T., Shi, C., Cave, E.R., et al.: Understanding selectivity for the electrochemical reduction of carbon dioxide to formic acid and carbon monoxide on metal electrodes. ACS Catal. **7**, 4822–4827 (2017). https://doi.org/10.1021/acscatal.7b00687
161. Nørskov, J.K., Bligaard, T., Rossmeisl, J., et al.: Towards the computational design of solid catalysts. Nat. Chem. **1**, 37–46 (2009). https://doi.org/10.1038/nchem.121
162. Strmcnik, D., Uchimura, M., Wang, C., et al.: Improving the hydrogen oxidation reaction rate by promotion of hydroxyl adsorption. Nat. Chem. **5**, 300–306 (2013). https://doi.org/10.1038/nchem.1574
163. Cheng, T., Wang, L., Merinov, B.V., et al.: Explanation of dramatic pH-dependence of hydrogen binding on noble metal electrode: greatly weakened water adsorption at high pH. J. Am. Chem. Soc. **140**, 7787–7790 (2018). https://doi.org/10.1021/jacs.8b04006
164. Hori, Y., Takahashi, R., Yoshinami, Y., et al.: Electrochemical reduction of CO at a copper electrode. J. Phys. Chem. B **101**, 7075–7081 (1997). https://doi.org/10.1021/jp970284i
165. Kim, C., Bui, J.C., Luo, X.Y., et al.: Tailored catalyst microenvironments for CO_2 electroreduction to multicarbon products on copper using bilayer ionomer coatings. Nat. Energy **6**, 1026–1034 (2021). https://doi.org/10.1038/s41560-021-00920-8
166. Unlu, M., Zhou, J.F., Kohl, P.A.: Anion exchange membrane fuel cells: experimental comparison of hydroxide and carbonate conductive ions. Electrochem. Solid State Lett. **12**, B27 (2009). https://doi.org/10.1149/1.3058999
167. Pătru, A., Binninger, T., Pribyl, B., et al.: Design principles of bipolar electrochemical co-electrolysis cells for efficient reduction of carbon dioxide from gas phase at low temperature. J. Electrochem. Soc. **166**, F34–F43 (2019). https://doi.org/10.1149/2.1221816jes
168. Rabinowitz, J.A., Kanan, M.W.: The future of low-temperature carbon dioxide electrolysis depends on solving one basic problem. Nat. Commun. **11**, 5231 (2020). https://doi.org/10.1038/s41467-020-19135-8
169. Keith, D.W., Holmes, G., St Angelo, D., et al.: A process for capturing CO_2 from the atmosphere. Joule **2**, 1573–1594 (2018). https://doi.org/10.1016/j.joule.2018.05.006
170. Sisler, J., Khan, S., Ip, A.H., et al.: Ethylene electrosynthesis: a comparative techno-economic analysis of alkaline vs membrane electrode assembly vs CO_2–CO–C_2H_4 tandems. ACS Energy Lett. **6**, 997–1002 (2021). https://doi.org/10.1021/acsenergylett.0c02633
171. Bohra, D., Chaudhry, J.H., Burdyny, T., et al.: Modeling the electrical double layer to understand the reaction environment in a CO_2 electrocatalytic system. Energy Environ. Sci. **12**, 3380–3389 (2019). https://doi.org/10.1039/C9EE02485A
172. Ziv, N., Mustain, W.E., Dekel, D.R.: The effect of ambient carbon dioxide on anion-exchange membrane fuel cells. Chemsuschem **11**, 1136–1150 (2018). https://doi.org/10.1002/cssc.201702330
173. Ziv, N., Dekel, D.R.: A practical method for measuring the true hydroxide conductivity of anion exchange membranes. Electrochem. Commun. **88**, 109–113 (2018). https://doi.org/10.1016/j.elecom.2018.01.021
174. Cao, X.Z., Novitski, D., Holdcroft, S.: Visualization of hydroxide ion formation upon electrolytic water splitting in an anion exchange membrane. ACS Mater. Lett. **1**, 362–366 (2019). https://doi.org/10.1021/acsmaterialslett.9b00195
175. Díaz-Sainz, G., Alvarez-Guerra, M., Solla-Gullón, J., et al.: Catalyst coated membrane electrodes for the gas phase CO_2 electroreduction to formate. Catal. Today **346**, 58–64 (2020). https://doi.org/10.1016/j.cattod.2018.11.073
176. Ashdot, A., Kattan, M., Kitayev, A., et al.: Design strategies for alkaline exchange membrane-electrode assemblies: optimization for fuel cells and electrolyzers. Membranes **11**, 686 (2021). https://doi.org/10.3390/membranes11090686
177. Díaz-Sainz, G., Alvarez-Guerra, M., Irabien, A.: Continuous electrochemical reduction of CO_2 to formate: comparative study of the influence of the electrode configuration with Sn and Bi-based electrocatalysts. Molecules **25**, 4457 (2020). https://doi.org/10.3390/molecules25194457
178. Li, Y.C., Yan, Z.F., Hitt, J., et al.: Bipolar membranes inhibit product crossover in CO_2 electrolysis cells. Adv. Sustain. Syst. **2**, 1700187 (2018). https://doi.org/10.1002/adsu.201700187
179. Lim, J., Kang, P.W., Jeon, S.S., et al.: Electrochemically deposited Sn catalysts with dense tips on a gas diffusion electrode for electrochemical CO_2 reduction. J. Mater. Chem. A **8**, 9032–9038 (2020). https://doi.org/10.1039/D0TA00569J

180. Yang, H.Z., Kaczur, J.J., Sajjad, S.D., et al.: CO_2 conversion to formic acid in a three compartment cell with Sustainion™ membranes. ECS Trans. **77**, 1425–1431 (2017). https://doi.org/10.1149/07711.1425ecst
181. Papakonstantinou, P., Deimede, V.: Self-cross-linked quaternary phosphonium based anion exchange membranes: assessing the influence of quaternary phosphonium groups on alkaline stability. RSC Adv. **6**, 114329–114343 (2016). https://doi.org/10.1039/C6RA24102F
182. Thomas, O.D., Soo, K.J.W.Y., Peckham, T.J., et al.: A stable hydroxide-conducting polymer. J. Am. Chem. Soc. **134**, 10753–10756 (2012). https://doi.org/10.1021/ja303067t
183. Wright, A.G., Holdcroft, S.: Hydroxide-stable ionenes. ACS Macro Lett. **3**, 444–447 (2014). https://doi.org/10.1021/mz500168d
184. Long, H., Pivovar, B.: Hydroxide degradation pathways for imidazolium cations: a DFT study. J. Phys. Chem. C **118**, 9880–9888 (2014). https://doi.org/10.1021/jp501362y
185. Hugar, K.M., KostalikCoates, H.A.G.W.: Imidazolium cations with exceptional alkaline stability: a systematic study of structure-stability relationships. J. Am. Chem. Soc. **137**, 8730–8737 (2015). https://doi.org/10.1021/jacs.5b02879
186. Fan, J.T., Wright, A.G., Britton, B., et al.: Cationic polyelectrolytes, stable in 10 M KOH_{aq} at 100 °C. ACS Macro Lett. **6**, 1089–1093 (2017). https://doi.org/10.1021/acsmacrolett.7b00679
187. Fan, J.T., Willdorf-Cohen, S., Schibli, E.M., et al.: Poly(bis-arylimidazoliums) possessing high hydroxide ion exchange capacity and high alkaline stability. Nat. Commun. **10**, 2306 (2019). https://doi.org/10.1038/s41467-019-10292-z
188. Mustain, W.E., Chatenet, M., Page, M., et al.: Durability challenges of anion exchange membrane fuel cells. Energy Environ. Sci. **13**, 2805–2838 (2020). https://doi.org/10.1039/D0EE01133A
189. Müller, J., Zhegur, A., Krewer, U., et al.: Practical ex-situ technique to measure the chemical stability of anion-exchange membranes under conditions simulating the fuel cell environment. ACS Mater. Lett. **2**, 168–173 (2020). https://doi.org/10.1021/acsmaterialslett.9b00418
190. Yang, K.L., Kas, R., Smith, W.A., et al.: Role of the carbon-based gas diffusion layer on flooding in a gas diffusion electrode cell for electrochemical CO_2 reduction. ACS Energy Lett. **6**, 33–40 (2021). https://doi.org/10.1021/acsenergylett.0c02184
191. Münchinger, A., Kreuer, K.D.: Selective ion transport through hydrated cation and anion exchange membranes. I. The effect of specific interactions. J. Membr. Sci. **592**, 117372 (2019)
192. Geise, G.M., Hickner, M.A., Logan, B.E.: Ionic resistance and permselectivity tradeoffs in anion exchange membranes. ACS Appl. Mater. Interfaces **5**, 10294–10301 (2013). https://doi.org/10.1021/am403207w
193. Xu, Y., Edwards, J.P., Liu, S.J., et al.: Self-cleaning CO_2 reduction systems: unsteady electrochemical forcing enables stability. ACS Energy Lett. **6**, 809–815 (2021). https://doi.org/10.1021/acsenergylett.0c02401
194. Varcoe, J.R., Slade, R.C.T.: Prospects for alkaline anion-exchange membranes in low temperature fuel cells. Fuel Cells **5**, 187–200 (2005). https://doi.org/10.1002/fuce.200400045
195. Overton, P., Li, W., Cao, X.Z., et al.: Tuning ion exchange capacity in hydroxide-stable poly(arylimidazolium) ionenes: increasing the ionic content decreases the dependence of conductivity and hydration on temperature and humidity. Macromolecules **53**, 10548–10560 (2020). https://doi.org/10.1021/acs.macromol.0c02014
196. Ozden, A., Wang, Y.H., Li, F.W., et al.: Cascade CO_2 electroreduction enables efficient carbonate-free production of ethylene. Joule **5**, 706–719 (2021). https://doi.org/10.1016/j.joule.2021.01.007
197. Mayerhöfer, B., McLaughlin, D., Böhm, T., et al.: Bipolar membrane electrode assemblies for water electrolysis. ACS Appl. Energy Mater. **3**, 9635–9644 (2020). https://doi.org/10.1021/acsaem.0c01127
198. Peugeot, A., Creissen, C.E., Schreiber, M.W., et al.: Advancing the anode compartment for energy efficient CO_2 reduction at neutral pH. ChemElectroChem **8**, 2726–2736 (2021). https://doi.org/10.1002/celc.202100742
199. De Mot, B., Hereijgers, J., Daems, N., et al.: Insight in the behavior of bipolar membrane equipped carbon dioxide electrolyzers at low electrolyte flowrates. Chem. Eng. J. **428**, 131170 (2022). https://doi.org/10.1016/j.cej.2021.131170
200. Yan, Z.F., Hitt, J.L., Zeng, Z.C., et al.: Improving the efficiency of CO_2 electrolysis by using a bipolar membrane with a weak-acid cation exchange layer. Nat. Chem. **13**, 33–40 (2021). https://doi.org/10.1038/s41557-020-00602-0
201. Luo, J.S., Vermaas, D.A., Bi, D.Q., et al.: Bipolar membrane-assisted solar water splitting in optimal pH. Adv. Energy Mater. **6**, 1600100 (2016). https://doi.org/10.1002/aenm.201600100
202. Huang, C.H., Xu, T.W.: Electrodialysis with bipolar membranes for sustainable development. Environ. Sci. Technol. **40**, 5233–5243 (2006). https://doi.org/10.1021/es060039p
203. Chen, Y.Y., Vise, A., Klein, W.E., et al.: A robust, scalable platform for the electrochemical conversion of CO_2 to formate: identifying pathways to higher energy efficiencies. ACS Energy Lett. **5**, 1825–1833 (2020). https://doi.org/10.1021/acsenergylett.0c00860
204. Peng, S.K., Xu, X., Lu, S.F., et al.: A self-humidifying acidic–alkaline bipolar membrane fuel cell. J. Power Sources **299**, 273–279 (2015). https://doi.org/10.1016/j.jpowsour.2015.08.104
205. Chen, Y.Y., Wrubel, J.A., Klein, W.E., et al.: High-performance bipolar membrane development for improved water dissociation. ACS Appl. Polym. Mater. **2**, 4559–4569 (2020). https://doi.org/10.1021/acsapm.0c00653
206. Balster, J., Srinkantharajah, S., Sumbharaju, R., et al.: Tailoring the interface layer of the bipolar membrane. J. Membr. Sci. **365**, 389–398 (2010). https://doi.org/10.1016/j.memsci.2010.09.034
207. Ge, Z.J., Shehzad, M.A., Yang, X.Q., et al.: High-performance bipolar membrane for electrochemical water electrolysis. J. Membr. Sci. **656**, 120660 (2022). https://doi.org/10.1016/j.memsci.2022.120660
208. McDonald, M.B., Freund, M.S.: Graphene oxide as a water dissociation catalyst in the bipolar membrane interfacial layer. ACS Appl. Mater. Interfaces **6**, 13790–13797 (2014). https://doi.org/10.1021/am503242v
209. Strathmann, H., Krol, J.J., Rapp, H.J., et al.: Limiting current density and water dissociation in bipolar membranes. J. Membr. Sci. **125**, 123–142 (1997). https://doi.org/10.1016/S0376-7388(96)00185-8
210. Vermaas, D.A., Wiegman, S., Nagaki, T., et al.: Ion transport mechanisms in bipolar membranes for (photo)electrochemical water splitting. Sustain. Energy Fuels **2**, 2006–2015 (2018). https://doi.org/10.1039/C8SE00118A
211. Donnan, F.G.: The theory of membrane equilibria. Chem. Rev. **1**, 73–90 (1924). https://doi.org/10.1021/cr60001a003
212. Tufa, R.A., Blommaert, M.A., Chanda, D., et al.: Bipolar membrane and interface materials for electrochemical energy systems. ACS Appl. Energy Mater. **4**, 7419–7439 (2021). https://doi.org/10.1021/acsaem.1c01140
213. Vermaas, D.A., Sassenburg, M., Smith, W.A.: Photo-assisted water splitting with bipolar membrane induced pH gradients for practical solar fuel devices. J. Mater. Chem. A **3**, 19556–19562 (2015). https://doi.org/10.1039/C5TA06315A

214. Sun, K., Liu, R., Chen, Y.K., et al.: A stabilized, intrinsically safe, 10% efficient, solar-driven water-splitting cell incorporating earth-abundant electrocatalysts with steady-state pH gradients and product separation enabled by a bipolar membrane. Adv. Energy Mater. **6**, 1600379 (2016). https://doi.org/10.1002/aenm.201600379
215. Hohenadel, A., Gangrade, A.S., Holdcroft, S.: Spectroelectrochemical detection of water dissociation in bipolar membranes. ACS Appl. Mater. Interfaces **13**, 46125–46133 (2021). https://doi.org/10.1021/acsami.1c12544
216. Shen, C.H., Wycisk, R., Pintauro, P.N.: High performance electrospun bipolar membrane with a 3D junction. Energy Environ. Sci. **10**, 1435–1442 (2017). https://doi.org/10.1039/C7EE00345E
217. Mel'nikov, S.S., Shapovalova, O.V., Shel'deshov, N.V., et al.: Effect of d-metal hydroxides on water dissociation in bipolar membranes. Petroleum Chem. **51**, 577–584 (2011)
218. Oda, Y., Yawataya, T.: Neutrality-disturbance phenomenon of membrane-solution systems. Desalination **5**, 129–138 (1968). https://doi.org/10.1016/S0011-9164(00)80208-8
219. Rajesh, A.M., Chakrabarty, T., Prakash, S., et al.: Effects of metal alkoxides on electro-assisted water dissociation across bipolar membranes. Electrochim. Acta **66**, 325–331 (2012). https://doi.org/10.1016/j.electacta.2012.01.102
220. Li, T.F., Lees, E.W., Goldman, M., et al.: Electrolytic conversion of bicarbonate into CO in a flow cell. Joule **3**, 1487–1497 (2019). https://doi.org/10.1016/j.joule.2019.05.021
221. Mandal, M.: Highly efficient bipolar membrane CO_2 electrolysis. ChemElectroChem **8**, 1448–1450 (2021). https://doi.org/10.1002/celc.202100243
222. Pribyl-Kranewitter, B., Beard, A., Schuler, T., et al.: Investigation and optimisation of operating conditions for low-temperature CO_2 reduction to CO in a forward-bias bipolar-membrane electrolyser. J. Electrochem. Soc. **168**, 043506 (2021). https://doi.org/10.1149/1945-7111/abf063
223. Panha, K., Fowler, M., Yuan, X.Z., et al.: Accelerated durability testing via reactants relative humidity cycling on PEM fuel cells. Appl. Energy **93**, 90–97 (2012). https://doi.org/10.1016/j.apenergy.2011.05.011
224. Giesbrecht, P.K., Freund, M.S.: Recent advances in bipolar membrane design and applications. Chem. Mater. **32**, 8060–8090 (2020). https://doi.org/10.1021/acs.chemmater.0c02829
225. Muroyama, A.P., Pătru, A., Gubler, L.: Review: CO_2 separation and transport via electrochemical methods. J. Electrochem. Soc. **167**, 133504 (2020). https://doi.org/10.1149/1945-7111/abbbb9
226. Oener, S.Z., Twight, L.P., Lindquist, G.A., et al.: Thin cation-exchange layers enable high-current-density bipolar membrane electrolyzers via improved water transport. ACS Energy Lett. **6**, 1–8 (2021). https://doi.org/10.1021/acsenergylett.0c02078
227. Dege, G.J. Chlanda, F.P. Lee, L.T.C., et al.: Method of making novel two component bipolar ion exchange membranes. US Patent 4,253,900, 3 Mar 1981
228. Pan, J.F., Hou, L.X., Wang, Q.Y., et al.: Preparation of bipolar membranes by electrospinning. Mater. Chem. Phys. **186**, 484–491 (2017). https://doi.org/10.1016/j.matchemphys.2016.11.023
229. Powers, D., Mondal, A.N., Yang, Z.Z., et al.: Freestanding bipolar membranes with an electrospun junction for high current density water splitting. ACS Appl. Mater. Interfaces **14**, 36092–36104 (2022). https://doi.org/10.1021/acsami.2c07680
230. Blommaert, M.A., Aili, D., Tufa, R.A., et al.: Insights and challenges for applying bipolar membranes in advanced electrochemical energy systems. ACS Energy Lett. **6**, 2539–2548 (2021). https://doi.org/10.1021/acsenergylett.1c00618
231. Garza, A.J., Bell, A.T., Head-Gordon, M.: Mechanism of CO_2 reduction at copper surfaces: pathways to C_2 products. ACS Catal. **8**, 1490–1499 (2018). https://doi.org/10.1021/acscatal.7b03477
232. Ozden, A., Liu, Y.J., Dinh, C.T., et al.: Gold adparticles on silver combine low overpotential and high selectivity in electrochemical CO_2 conversion. ACS Appl. Energy Mater. **4**, 7504–7512 (2021). https://doi.org/10.1021/acsaem.1c01577
233. Chen, B.T., Li, B.R., Tian, Z.Q., et al.: Enhancement of mass transfer for facilitating industrial-level CO_2 electroreduction on atomic $Ni–N_4$ sites. Adv. Energy Mater. **11**, 2102152 (2021). https://doi.org/10.1002/aenm.202102152
234. Wang, Q.Y., Liu, K., Fu, J.W., et al.: Atomically dispersed s-block magnesium sites for electroreduction of CO_2 to CO. Angew. Chem. Int. Ed. **60**, 25241–25245 (2021). https://doi.org/10.1002/anie.202109329
235. Chae, S.Y., Lee, S.Y., Joo, O.S.: Directly synthesized silver nanoparticles on gas diffusion layers by electrospray pyrolysis for electrochemical CO_2 reduction. Electrochim. Acta **303**, 118–124 (2019). https://doi.org/10.1016/j.electacta.2019.02.046
236. Dinh, C.T., García de Arquer, F.P., Sinton, D., et al.: High rate, selective, and stable electroreduction of CO_2 to CO in basic and neutral media. ACS Energy Lett. **3**, 2835–2840 (2018). https://doi.org/10.1021/acsenergylett.8b01734
237. Qi, Z., Biener, M.M., Kashi, A.R., et al.: Electrochemical CO_2 to CO reduction at high current densities using a nanoporous gold catalyst. Mater. Res. Lett. **9**, 99–104 (2021). https://doi.org/10.1080/21663831.2020.1842534
238. Wei, S.T., Zou, H.Y., Rong, W.F., et al.: Conjugated nickel phthalocyanine polymer selectively catalyzes CO_2-to-CO conversion in a wide operating potential window. Appl. Catal. B Environ. **284**, 119739 (2021). https://doi.org/10.1016/j.apcatb.2020.119739
239. Salvatore, D.A., Weekes, D.M., He, J.F., et al.: Electrolysis of gaseous CO_2 to CO in a flow cell with a bipolar membrane. ACS Energy Lett. **3**, 149–154 (2018). https://doi.org/10.1021/acsenergylett.7b01017
240. Yang, K.L., Li, M.R., Subramanian, S., et al.: Cation-driven increases of CO_2 utilization in a bipolar membrane electrode assembly for CO_2 electrolysis. ACS Energy Lett. **6**, 4291–4298 (2021). https://doi.org/10.1021/acsenergylett.1c02058
241. Li, Y.C., Lee, G., Yuan, T.G., et al.: CO_2 electroreduction from carbonate electrolyte. ACS Energy Lett. **4**, 1427–1431 (2019). https://doi.org/10.1021/acsenergylett.9b00975
242. Blommaert, M.A., Sharifian, R., Shah, N.U., et al.: Orientation of a bipolar membrane determines the dominant ion and carbonic species transport in membrane electrode assemblies for CO_2 reduction. J. Mater. Chem. A Mater. **9**, 11179–11186 (2021). https://doi.org/10.1039/d0ta12398f
243. Fan, T.T., Ma, W.C., Xie, M.C., et al.: Achieving high current density for electrocatalytic reduction of CO_2 to formate on bismuth-based catalysts. Cell Rep. Phys. Sci. **2**, 100353 (2021). https://doi.org/10.1016/j.xcrp.2021.100353
244. Grigioni, I., Sagar, L.K., Li, Y.C., et al.: CO_2 electroreduction to formate at a partial current density of 930 mA cm^{-2} with InP colloidal quantum dot derived catalysts. ACS Energy Lett. **6**, 79–84 (2021). https://doi.org/10.1021/acsenergylett.0c02165
245. Li, J., Jiao, J.Q., Zhang, H.C., et al.: Two-dimensional SnO_2 nanosheets for efficient carbon dioxide electroreduction to formate. ACS Sustainable Chem. Eng. **8**, 4975–4982 (2020). https://doi.org/10.1021/acssuschemeng.0c01070
246. Fan, L., Xia, C., Zhu, P., et al.: Electrochemical CO_2 reduction to high-concentration pure formic acid solutions in an all-solid-state reactor. Nat. Commun. **11**, 3633 (2020). https://doi.org/10.1038/s41467-020-17403-1
247. Yang, J., Wang, X.L., Qu, Y.T., et al.: Bi-based metal-organic framework derived leafy bismuth nanosheets for carbon dioxide electroreduction. Adv. Energy Mater. **10**, 2001709 (2020). https://doi.org/10.1002/aenm.202001709

248. Gong, Q.F., Ding, P., Xu, M.Q., et al.: Structural defects on converted bismuth oxide nanotubes enable highly active electrocatalysis of carbon dioxide reduction. Nat. Commun. **10**, 2807 (2019). https://doi.org/10.1038/s41467-019-10819-4
249. Liu, H., Su, Y.Q., Kuang, S.Y., et al.: Highly efficient CO_2 electrolysis within a wide operation window using octahedral tin oxide single crystals. J. Mater. Chem. A **9**, 7848–7856 (2021). https://doi.org/10.1039/D1TA00285F
250. Zhao, Y., Liu, X.L., Liu, Z.X., et al.: Spontaneously Sn-doped Bi/BiO_x core–shell nanowires toward high-performance CO_2 electroreduction to liquid fuel. Nano Lett. **21**, 6907–6913 (2021). https://doi.org/10.1021/acs.nanolett.1c02053
251. Díaz-Sainz, G., Alvarez-Guerra, M., Irabien, A.: Continuous electroreduction of CO_2 towards formate in gas-phase operation at high current densities with an anion exchange membrane. J. CO2 Util. **56**, 1018 (2022)
252. Bienen, F.B., Kopljar, D., Löwe, A., et al.: Utilizing formate as an energy carrier by coupling CO_2 electrolysis with fuel cell devices. Chemie Ingenieur Tech. **91**, 872–882 (2019). https://doi.org/10.1002/cite.201800212
253. Xing, Z., Hu, X., Feng, X.F.: Tuning the microenvironment in gas-diffusion electrodes enables high-rate CO_2 electrolysis to formate. ACS Energy Lett. **6**, 1694–1702 (2021). https://doi.org/10.1021/acsenergylett.1c00612
254. He, S.S., Ni, F.L., Ji, Y.J., et al.: The p-orbital delocalization of main-group metals to boost CO_2 electroreduction. Angew. Chem. Int. Ed. **57**, 16114–16119 (2018). https://doi.org/10.1002/anie.201810538
255. Sen, S., Skinn, B., Hall, T., et al.: Pulsed electrodeposition of tin electrocatalysts onto gas diffusion layers for carbon dioxide reduction to formate. MRS Adv. **2**, 451–458 (2017). https://doi.org/10.1557/adv.2016.652
256. Díaz-Sainz, G., Alvarez-Guerra, M., Solla-Gullón, J., et al.: CO_2 electroreduction to formate: continuous single-pass operation in a filter-press reactor at high current densities using Bi gas diffusion electrodes. J. CO2 Util. **34**, 12–19 (2019). https://doi.org/10.1016/j.jcou.2019.05.035
257. Wang, Z.T., Qi, R.J., Liu, D.Y., et al.: Exfoliated ultrathin $ZnIn_2S_4$ nanosheets with abundant zinc vacancies for enhanced CO_2 electroreduction to formate. Chemsuschem **14**, 852–859 (2021). https://doi.org/10.1002/cssc.202002785
258. Deng, P.L., Yang, F., Wang, Z.T., et al.: Metal-organic framework-derived carbon nanorods encapsulating bismuth oxides for rapid and selective CO_2 electroreduction to formate. Angew. Chem. Int. Ed. **59**, 10807–10813 (2020). https://doi.org/10.1002/anie.202000657
259. Xia, C., Zhu, P., Jiang, Q., et al.: Continuous production of pure liquid fuel solutions via electrocatalytic CO_2 reduction using solid-electrolyte devices. Nat. Energy **4**, 776–785 (2019). https://doi.org/10.1038/s41560-019-0451-x
260. Díaz-Sainz, G., Alvarez-Guerra, M., Solla-Gullón, J., et al.: Gas–liquid–solid reaction system for CO_2 electroreduction to formate without using supporting electrolyte. Aiche J. **66**, e16299 (2020). https://doi.org/10.1002/aic.16299
261. Del Castillo, A., Alvarez-Guerra, M., Solla-Gullón, J., et al.: Sn nanoparticles on gas diffusion electrodes: synthesis, characterization and use for continuous CO_2 electroreduction to formate. J. CO2 Util. **18**, 222–228 (2017). https://doi.org/10.1016/j.jcou.2017.01.021
262. Kopljar, D., Inan, A., Vindayer, P., et al.: Electrochemical reduction of CO_2 to formate at high current density using gas diffusion electrodes. J. Appl. Electrochem. **44**, 1107–1116 (2014)
263. Pavesi, D., van de Poll, R.C.J., Krasovic, J.L., et al.: Cathodic disintegration as an easily scalable method for the production of Sn- and Pb-based catalysts for CO_2 reduction. ACS Sustain. Chem. Eng. **8**, 15603–15610 (2020). https://doi.org/10.1021/acssuschemeng.0c04875
264. Fujinuma, N., Lofland, S.: Acid-compatible catalyst development and machine-learning-assisted cell optimization toward cost-effective CO_2 reduction reaction: Co-P4VP-derived catalyst and Nafion-based membrane electrode assembly. Meet. Abstr. (2021). https://doi.org/10.1149/ma2021-02281848mtgabs
265. Cao, C.S., Ma, D.D., Gu, J.F., et al.: Metal-organic layers leading to atomically thin bismuthene for efficient carbon dioxide electroreduction to liquid fuel. Angew. Chem. Int. Ed. **59**, 15014–15020 (2020). https://doi.org/10.1002/anie.202005577
266. Wang, D., Liu, C.W., Zhang, Y.N., et al.: CO_2 electroreduction to formate at a partial current density up to 590 mA mg^{-1} via micrometer-scale lateral structuring of bismuth nanosheets. Small **17**, e2100602 (2021). https://doi.org/10.1002/smll.202100602
267. Lou, Y.Y., Fu, D., Fabre, B., et al.: Bismuth coated graphite felt modified by silver particles for selective electroreduction of CO_2 into formate in a flow cell. Electrochimica Acta **371**, 137821 (2021). https://doi.org/10.1016/j.electacta.2021.137821
268. Zhao, F.: Exploring electrochemical flow-cell designs and parameters for CO_2 reduction to formate under industrially relevant conditions. J. Electrochem. Soc. **169**, 054511 (2022). https://doi.org/10.1149/1945-7111/ac6bc1
269. Duan, G.Y., Li, X.Q., Ding, G.R., et al.: Highly efficient electrocatalytic CO_2 reduction to C_{2+} products on a poly(ionic liquid)-based Cu^0–Cu^I tandem catalyst. Angew. Chem. Int. Ed. **61**, e202110657 (2022). https://doi.org/10.1002/anie.202110657
270. Lu, J.N., Liu, J., Zhang, L., et al.: Crystalline mixed-valence copper supramolecular isomers for electroreduction of CO_2 to hydrocarbons. J. Mater. Chem. A **9**, 23477–23484 (2021). https://doi.org/10.1039/D1TA07148C
271. Zhao, X., Du, L.J., You, B., et al.: Integrated design for electrocatalytic carbon dioxide reduction. Catal. Sci. Technol. **10**, 2711–2720 (2020). https://doi.org/10.1039/D0CY00453G
272. Chen, X.Y., Chen, J.F., Alghoraibi, N.M., et al.: Electrochemical CO_2-to-ethylene conversion on polyamine-incorporated Cu electrodes. Nat. Catal. **4**, 20–27 (2021). https://doi.org/10.1038/s41929-020-00547-0
273. Liu, W.Q., Wei, S.L., Bai, P.Y., et al.: Robust coal matrix intensifies electron/substrate interaction of nickel–nitrogen (Ni–N) active sites for efficient CO_2 electroreduction at industrial current density. Appl. Catal. B Environ. **299**, 120661 (2021). https://doi.org/10.1016/j.apcatb.2021.120661
274. Kutz, R.B., Chen, Q.M., Yang, H.Z., et al.: Sustainion imidazolium-functionalized polymers for carbon dioxide electrolysis. Energy Technol. **5**, 929–936 (2017). https://doi.org/10.1002/ente.201600636

Faezeh Habibzadeh received her Ph.D. degree in inorganic chemistry from Michigan State University, where she worked on the electrocatalytic oxidation of ammonia under mild conditions. After graduation, Dr. Habibzadeh continued her work in the field of electrocatalysis at the University of British Columbia in Prof. Berlinguette's research group and the National Research Council of Canada (NRC). Dr. Habibzadeh's research interests include CO_2 capture and electrolysis, development and evaluation of electrocatalyst materials, characterization of anion exchange membranes, and accelerated material discovery.

Peter Mardle is a Research Assistant at the Energy, Mining and Environment Research Centre for the National Research Council of Canada (NRC). He received his MChem from the University of Southampton, UK, in 2015. In 2020, he received a Ph.D. from the University of Birmingham, UK, as part of the Engineering and Physical Sciences Research Council's (EPSRC) Centre for Doctoral Training in Fuel Cells and their Fuels. Dr. Mardle then joined Prof. Holdcroft's group as a postdoctoral researcher at Simon Fraser University, Canada, until 2022. He has expertise in catalyst and ionomer material development and electrochemical characterization for proton exchange membrane fuel cells, CO_2 electrolyzers and alkaline exchange membrane water electrolyzers.

Nana Zhao received her Ph.D. degree in Polymer Chemistry and Physics at the Changchun Institute of Applied Chemistry, Chinese Academy of Sciences, in 2008. After obtaining her Ph.D. degree, she joined Prof. Ting Xu's group as a postdoctoral fellow to carry out research on polymer membranes in Materials Science and Engineering at the University of California, Berkeley, USA. Upon completing one term of postdoctoral research, she took a position as a research associate at the National Research Council of Canada – Energy, Mining and Environment Portfolio (NRCEME, formerly the NRC Institute for Fuel Cell Innovation) for two years. In 2013, she joined Vancouver International Clean-Tech Research Institute Inc. (VICTRII) as a research scientist. Since joining NRC as a Research Officer in 2015, Dr. Zhao has been working on polymer materials and polymer membranes in the application of electrochemical energy conversion devices, including proton exchange membrane fuel cell (PEMFC), vanadium redox flow battery (VRFB), polymer electrolyte membrane electrolysis and electrochemical reduction of carbon dioxide. These research activities involve synthesis, evaluation and characterization of ionomer and polymer membranes; membrane performance and durability testing and diagnosis; membrane electrode assembly (MEA) design and fabrication; MEA defects for quality control (QC) of PEMFC and water electrolyzer components. Dr. Zhao has coauthored more than 30 research papers published in peer-reviewed journals, coedited one book related to PEM water electrolysis and eight granted patents.

Harry D. Riley is an undergraduate student at the University of British Columbia (UBC), studying Materials Engineering. He will graduate in 2024 with a Bachelor degree of Applied Science and hopes to move into the automotive field. He worked at National Research Canada during 2020–2021 as a co-op student on material characterization for vanadium redox flow batteries and CO_2 electrolysis. Currently, he is the captain of Formula UBC Racing, an engineering design team at UBC, working on understanding the heat transfer due to stress by modelling using the finite element analysis in the Abaqus CAE software.

Danielle A. Salvatore completed her Ph.D. in the Berlinguette group at UBC in 2020. She received her M.A.Sc. degree in Chemical and Biological Engineering from UBC in 2015 and her B.Sc. in Chemistry from McGill University in 2013. Her research interests include CO_2 electrolyzer design and optimization.

Curtis P. Berlinguette leads a multidisciplinary team at the University of British Columbia that designs and builds electrochemical reactors to power the planet. These reactors are designed to use electricity to: (i) convert CO_2 into fuels and products; (ii) decarbonize the built environment; and (iii) upgrade commodity chemicals. Dr. Berlinguette is a Distinguished University Scholar at UBC, a Fellow of the Royal Society of Canada, and a CIFAR Program Director.

Steven Holdcroft is a Professor of Chemistry at Simon Fraser, Canada Research Chair, former Departmental Chair and Past President of the Canadian Society for Chemistry. He researches materials for electrochemical energy conversion & storage. He is the author of 300 peer-reviewed articles. He was a board of director of the Canadian Fuel Cell and Hydrogen Association for over 10 years. Dr. Holdcroft has received the Macromolecular Science and Engineering Division Award of the Chemical Institute of Canada and the Canadian Society of Canada RioTinto Alcan Award for electrochemistry. He was elected to the fellowship of the Royal Society of Canada in 2021.

Zhiqing Shi is a Senior Research Officer in Energy, Mining and Environment Research Centre at National Research Council Canada (NRC). He received his B.Eng. and M.Sc. degrees from the East China University of Chemical Technology, Ph.D. degree from Simon Fraser University. His research career started as early as in 1987 at Shanghai 3F New Materials Co., Ltd. (Shanghai, China) on fluoropolymer synthesis. Dr. Shi joined at NRC in 2002 and has extended his research interest from polymer synthesis into ion exchange membranes for PEM fuel cells, and recently for other clean energy applications such as vanadium redox flow battery (VRFB), CO_2 electrolyzers, and water electrolyzers. As a well recognized expert in ion exchange membranes with traceable impacts on the Canadian industry, his expertise has been consistently demonstrated through leading a significant number of sizable projects collaborating with universities, industries, and governments, nationally and internationally.